THE NUMERICAL MODELING OF PARTICLE DISPERSION IN TURBULENT SHEAR FLOWS

THE NUMERICAL MODELING OF PARTICLE DISPERSION IN TURBULENT SHEAR FLOWS

By

DOUGLAS ROBERT EVINOU, B.ENG. (Mechanical Engineering)
McMaster University, Hamilton, Ontario, Canada

A Thesis
Submitted to the School of Graduate Studies
in Partial Fulfilment of the Requirements
for the Degree
Master of Applied Science

McMaster University

MASTER OF APPLIED SCIENCE (2003) McMaster University
(Mechanical Engineering) Hamilton, Ontario

TITLE:	The Numerical Modeling of Particle Dispersion in Turbulent Shear Flows
AUTHOR:	Douglas Robert Evinou B.ENG. (Mechanical Engineering) McMaster University, Hamilton, Ontario, Canada
SUPERVISOR:	Dr. Marilyn F. Lightstone, Associate Professor Department of Mechanical Engineering McMaster University
NUMBER OF PAGES:	xiv, 100

Abstract

This thesis investigates Stochastic Separated Flow (SSF) models for particle dispersion in turbulent shear flows. A new model is presented that accounts for anisotropy and incorporates a temporal and a spatial autocorrelation in the description of the fluctuating component of the turbulent gas-phase velocity. This model and three SSF models available in the literature are evaluated by comparing predictions with the shear layer experiments of Lazaro and Lasheras (1989), Hishida et al (1992) and the turbulent round jet experiment of Yuu et al (1978). Results are discussed and deficiencies in the models explored. The new model of Evinou and Lightstone compensates for the crossing trajectory effect with the inclusion of a spatial correlation based on the relative velocity of the particle and the time step employed.

Contents

List of Figures

List of Tables

Nomenclature

Symbol	Definition
Greek	
δ_{ij}	Kronecker delta
δt	timestep
Δt	timestep
ϵ	turbulent diffusivity
μ	molecular dynamic viscosity
ν_t	turbulent kinematic viscosity
ρ_g	density of gas
ρ_p	density of particle
σ^2	variance
τ_p	particle relaxation time
τ_{LI}	Lagrangian integral timescale
θ	azimuthal coordinate

English	
C_D	drag coefficient
C_μ	eddy viscosity model proportionality constant
d_p	particle diameter
f	ratio of the drag coefficient to Stokes drag
k	turbulent kinetic energy
l_e	characteristic eddy length
m_p	particle mass
p	pressure
$R(\delta t)$	Lagrangian temporal correlation
Re	Reynolds number, $U_o D/\nu$

Re_p	Particle Reynolds number, $U_{REL}D_p/\nu$
t	time
t_e	eddy lifetime
t_{int}	particle interaction time
t_{tr}	transit time of a particle
u	instantaneous velocity
$\overline{U}$	mean velocity
$u^{'}$	velocity fluctuation
u_{REL}	relative velocity of the particle
x_i	distance in i direction

Subscripts

f	fluid
g	gas-phase
p	particle
t	time

CHAPTER 1

Introduction

Particle dispersion problems exist in a number of engineering fields, including the combustion of liquid-fuel sprays, the spread of pollutants and contaminants from exhaust systems, and many other industrial processes. In recent years, engineers have been interested in modeling these types of flows numerically. The models that have been developed in this field have grown in complexity and efficiency right alongside the development of the computer.

The main challenge in modelling particle motion in a turbulent flow is in correctly accounting for the effect of fluid turbulence on the particle trajectory. In tracking a particle in a Lagrangian framework, the instantaneous gas velocity has to be known at every particle location throughout the computational domain. Thus, engineers have designed complex Lagrangian frameworks that are built upon an Eulerian solution of the flow field using traditionally a $k-\epsilon$ framework, or in more complicated solutions, a Reynolds Stress Model.

A new model will be proposed that builds upon the strengths of the models found throughout the literature. Predictions will be generated and compared with classic shear flow experimental results, and assessed with reference to models used in industry.

The next chapter in this thesis will outline the work that has been done in particle dispersion modelling research in the past, and will detail the evolution of the solution

techniques to the present day. That will be followed by a chapter that explains the basic mathematical equations that are solved in turbulence modelling, and the techniques that are used to solve for particle trajectories. Chapter four will focus specifically on stochastic separated flow models, and will describe particular models of interest in great detail. As well, a new model will be introduced that is built on the promising models of Zhou & Leschziner and Berlemont *et al.* Chapters five through seven will each feature turbulent shear experiments that have been simulated to assess the performance of the stochastic separated flow models of Shuen *et al.*, Hennick & Lightstone, Zhou & Leschziner and the proposed model of Evinou and Lightstone. The results of these simulations will be discussed, and the merits and shortcomings of the models will be assessed. The work will be concluded with a summary of the research results and recommendations for future work.

CHAPTER 2

Background

This chapter will serve as an introduction to the nature of particle dispersion modeling as well as a review of the existing models from the literature. The chapter will begin with a description of the particle equation of motion introduced by Basset (1888), Boussinesq (1903) and Oseen (1927). This will be followed by an outline of the important physical phenomenon that make the particle dispersion problem unique, as well as the definition of a few key terms that will be used throughout the thesis.

Particle dispersion models can be broadly classified into two categories based on the type of reference frame used to model the particulate phase: Lagrangian or Eulerian. The two categories will be discussed and an introduction to some key models in both will be introduced. Particular focus will be given to Lagrangian models, since these models tend to be more applicable to a wider range of applications. Specific attention will be given to a specific subset of Lagrangian particle dispersion models, that being stochastic separated flow models.

2.1 Particle Equation of Motion

The particle equation of motion introduced by Basset, Boussinesq and Oseen (BBO) describes the motion of a particle at low Reynolds numbers through a flow field. For a spherical particle, the full equation has the form:

$$\frac{\pi}{6}d_p^3\rho_p\frac{dU_p}{dt} = 3\pi\mu d_p(U-U_p) - \frac{\pi}{6}d_p^3\nabla p + \frac{\pi}{12}d_p^3\rho\frac{d}{dt}(U-U_p) + \frac{3}{2}d_p^2\sqrt{\pi\rho\mu}\int_0^t \frac{\frac{d}{d\tau}(U-U_p)}{\sqrt{t-\tau}}d\tau + \sum_i f_i \quad (2.1)$$

The five terms on the right-hand side of the equation are, in order from left to right, the forces due to the Stokes drag, pressure gradient, added mass, Basset historic integral, and other external forces such as gravitational force and electrostatic force (Fan & Zhu,1998). When the density of a particle is much greater then the density of the fluid phase (i.e. $\rho_p >> \rho_g$), most of these effects can be shown to scale out of the problem, and the solution of the particle trajectories is a function of Stokes drag and gravitational forces only. The solution of the particle equation of motion will be discussed in great detail in section 3.4.

2.2 Particle Dispersion

Before embarking on a summary of different particle dispersion models available in the literature, it will be useful to briefly outline and define some important concepts in particle dispersion modeling.

The size of the particle relative to the length scales of turbulence is a key parameter in determining the nature of the dispersion. Particles are generally split into two categories: small and medium. A small particle's diameter is less then the Kolmogorov length scale of the carrier phase (i.e. the smallest eddy size). A medium-sized particle's diameter is in-between the Kolmogorov scale and the integral length scale of the flow (determined from the characteristic dimensions of the flow (e.g. wake size, jet diameter etc.). Large particles with diameters comparable to the integral length

scale do not appear in practical systems and hence will not be discussed in this thesis (Shirolkar *et al.*,1996).

The density of the particle relative to the density of the gaseous phase is another important consideration in particle dispersion. If the particle is significantly heavier than the carrier phase, it will not respond to the turbulent fluctuations of the fluid (also true for the diameter of the particle). This is known as the inertia effect, and it is characterized by the particle relaxation time. The particle relaxation time is defined as the rate of response of particle acceleration to the relative velocity between the particle and the carrier fluid (Shirolkar *et al.*,1996). The particle relaxation time is derived from the particle equation of motion for the case when $Re << 1$, and has the form:

$$\tau_p = \frac{\rho_p d_p^2}{18\mu} \tag{2.2}$$

A particle may or may not interact with an eddy for the entire lifetime of that eddy. The phenomenon of migration of a particle from one eddy to another is known as the crossing trajectory effect (CTE). This premature migration is due to the significant free fall velocity of the particle under consideration (i.e. gravity is important). The minimum time (t_c) a particle would take to cross an eddy with characteristic dimension l_e can be approximated by (as suggested by Gosman & Ioannides):

$$t_c = \frac{l_e}{v_d} \tag{2.3}$$

where the denominator is the magnitude of the relative velocity between the particle and the fluid. If the minimum crossing time were smaller then the eddy lifetime, the particle would jump to another eddy. Thus, it is possible to account for the CTE by allowing a particle to interact with an eddy for a time that is the minimum of

t_c and the lifetime of the eddy, t_e (Shirolkar *et al.*,1996). This phenomenon is most important when dealing with large, heavy particles.

2.3 Particle Dispersion Modeling

The modeling of dispersion of particles in a gaseous carrier phase is complex since it requires the modeling of two separate phases, the carrier phase and the particulate phase. The carrier phase is generally modeled in an Eulerian coordinate system using standard turbulence models such as the $k - \epsilon$ model. Researchers have consistently used this as a starting point in their work, but have diverged in a myriad of directions when deciding how to model the particulate phase.

There are many popular methods in use today to predict the dispersion of particles in turbulent flows. In order to predict how a particle will be dispersed in the carrier phase, knowledge of the instantaneous velocity fluctuations are required at all points along the particle's trajectory. Most dispersion models can be broadly classified based on the type of reference frame, Lagrangian or Eulerian, that is used to model the particulate phase. In the Eulerian framework, the particle phase is treated as a continuum and dispersion is calculated by solution of conservation equations for the particle and the gas phases. The Lagrangian models treat the particles as discrete entities, and solve individual particle equations of motions to generate trajectories and eventually dispersion data.

2.3.1 Eulerian Particle Dispersion Models

The turbulence models that are used in most flow field solutions (like the $k-\epsilon$ model for instance) are cast in an Eulerian framework. These models are essentially a set of partial differential equations that can be solved easily in a fixed reference frame (Shirolkar *et al.*,1996). It is therefore natural to construct a particle dispersion model, that is dependent on the fluid-phase solution, in an Eulerian reference frame as well. The challenge, then, is to develop a set of appropriate partial differential equations to model particle properties of interest, such as particle velocity and particle number density.

The main advantage of Eulerian models is that the same numerical methods that are used to solve the fluid-phase equations can be used to solve the particle equations. This leads to fast solutions at low computational cost. The penalty associated with this approach is the limiting assumption that is made in assuming a continuous particle field (Berlemont *et al.*,1990). For instance, there is no justification to model the turbulent dispersion by analogy to Fick's law, thus using an effective particle diffusivity (Shirolkar *et al.*,1996). The derivation of the steady-state continuity equation for average particle number density gives rise to the problematic term, Γ_P, termed the 'effective particle diffusivity', which is given by:

$$\Gamma_p = \frac{\mu_p^t}{\sigma_p^t} \tag{2.4}$$

where μ_p^t is the turbulent particle viscosity and σ_p^t is the turbulent particle Schmidt number. The problem arises since particles do not equilibrate with either local fluid or each other as they move through the flow field. As well, Eulerian approaches do not work well for dilute flows, which limits there applicability for many practical applications. Difficulty also arises from the application of boundary conditions in the

Eulerian model, since the particles and the fluid do not interact in the same manner at walls, for example. The equations of motions for the individual particles, which act independently of each other, are "parabolic and not directly amenable to elliptic-like boundary conditions" (Crowe *et al.*, 1996).

Key work in this area has been developed by researchers such as Durst *et al.* (1984), Elgobashi *et al.* (1984) and Picart *et al.* (1986).

2.3.2 Lagrangian Particle Dispersion Models

The Lagrangian reference frame is the natural frame for treating particles. This is because in this reference frame particles are treated as discrete objects, and their motion is tracked as they move through the flow field. In this way, it is possible to account for the noncontinuum behaviour of particles and the particle history effects. The particle trajectories of representative samples are obtained by solving the individual particle momentum equation through the Eulerian velocity field. Therefore, these models in general need to estimate the fluctuating component of the fluid velocity at every particle location as the particle moves in discrete time steps through the computational domain.

Examples of Lagrangian particle dispersion models will be outlined in great detail in the next section.

2.4 Stochastic Separated Flow Models

Stochastic separated flow (SSF) models use a Lagrangian framework to solve the trajectory equations of a particle as it interacts with a succession of discrete turbulent

eddies. First developed by Dukowicz (Gosman & Ioannides,1983), this Lagrangian framework treats the particles as distinct entities within the fluid phase. The solution is stochastic since the particle interacts with the instantaneous velocities of the gas-phase turbulence. The model incorporates the turbulent fluctuations by random sampling to determine the instantaneous velocity of the continuum gas-phase. More precisely, turbulent velocity fluctuations are determined from statistical correlations of such fluctuations. These models solve the particle equation of motion, which will be discussed in detail in section 3.4.

There are two main, distinct SSF models: discrete eddy models and correlated models.

2.4.1 Discrete Eddy Models

Discrete eddy models are the simplest of the SSF models. They model the fluid as a collection of discrete eddies, each with a constant velocity and finite life-time. The particles enter the eddies, and are subjected to the same instantaneous velocity of the eddy for the duration of the eddy-particle interaction. The interaction time is governed by either the time required for the particle to cross the eddy, or the lifetime of the eddy - depending on whether the crossing-trajectory effect or eddy capture dominates. Gosman & Ioannides (1983) and Shuen *et al.* (1983) are examples of discrete eddy models. These models remain, because of their simplicity and robustness, the primary schemes for predicting particle dispersion in most current commercial computational codes (Crowe *et al.*, 1996).

However, these types of models do have their limitations due to the simplifying assumptions inherent in them. Both of these models assume that $\overline{u'^2} = \overline{v'^2} = \overline{w'^2}$, and that each velocity u',v', and w' at a given point are independent of each other. Thus, isotropy of the turbulence is an inherent assumption in each of these models, a condition that is rare to find in most practical flows of interest. Second, the models

hold $u_g^{'}$ constant over the entire particle/eddy interaction time. In the next section, models will be described which attempt to compensate for these shortcomings.

2.4.2 Correlated Models

The discrete eddy models described in the previous section are founded on the hypothesis that a particle will be exposed to only one fluctuating velocity over the time it interacts with an eddy. Zhou & Leschziner were the first researchers to argue that it is more correct to assume that a particle will be exposed to a series of correlated gas-phase velocities over the course of the interaction period. Their model accounted for the temporal correlation of turbulent fluctuations by introducing an exponential function as suggested by Hinze (1975).

$$R(\delta t) = exp\left(-\frac{\delta t}{\tau_{LI}}\right) \tag{2.5}$$

where $\tau_{LI} = \gamma(C_\mu^{0.75}k^{1.5}/\epsilon)/(2/3k)^{0.5}$. Zhou & Leschziner took the value of γ as 0.8 based on an optimization carried out for isotropic turbulence.

Using this correlation, Zhou & Leschziner developed an expression for calculating a new turbulent velocity fluctuation.

$$u_t^{'} = R(\delta t)u_{t-\delta t}^{'} + e_t \tag{2.6}$$

where $u_t^{'}$ is the current gas-phase fluctuating velocity, $u_{t-\delta t}^{'}$ is the previous gas-phase fluctuating velocity, and e_t is an independent random variable intended to take into account randomness that can occur during the time step δt.

Subsequently, several researchers have built upon this idea, generating models which take into account anisotropy and directional correlation. Key amongst these researchers are Berlemont *et al.* and Burry & Bergeles. Their work will be outlined in detail in Chapter 4.

2.5 Summary

This section began with an outline of some of the key concepts in particle dispersion modelling. Such terms as the crossing-trajectory effect, particle relaxation numbers and particle residency where introduced to make clear the motivation behind many of the models found in the literature. The two main types of particle dispersion models were outlined, those being the Eulerian and the Lagrangian models. The differences between the two types of models were explored.

The different kinds of Lagrangian models that exist in the literature were then focused upon as these are the models that will be used in this thesis. Specifically, the difference between Discrete Eddy models and Correlated models were discussed. The models of Gosman & Ioannides and Shuen *et al.* are examples of discrete eddy models that are prevalent in industry and commercial CFD packages. However, these models do not take into account the anisotropy of many practical flows, and assume that a particle will only be exposed to one gas turbulent velocity fluctuation during the coarse of the particle-eddy interaction time.

The more physically correct correlated models were examined next. The key feature of these models is that they allow for a particle to see a series of correlated velocities while trapped inside an eddy, as opposed to only one characteristic velocity. The first example of a correlated model to be looked at was Zhou & Leschziner (1991b).

Several researchers have also attempted to account for anisotropy and directional correlations in their work. The finer details of the correlated models will be explored in Chapter 4, since the new model introduced in this thesis is directly derived from this work.

In the next chapter, the numerical and computational solution methods for particle dispersion will be discussed.

CHAPTER 3

Mathematical Models

This chapter will outline the mathematics behind Eulerian-Lagrangian particle dispersion models, and particularly the numerical modeling methods used for both the fluid and the particulate phases. As with most investigations into fluid-dynamic phenomenon, it is instructive to begin by looking at the Navier-Stokes equations that govern the fluid phase, and the method of decomposition that is utilized when flows are turbulent. The different computational turbulence closure models will be studied in some detail, specifically the $k-\epsilon$ model and the second order closure models, which are two of the more popular turbulence models found in the literature.

The focus of the chapter will then shift to the mathematical models that govern the particulate phase in the particle dispersion models studied in this thesis. The derivation and physics behind the particle equation of motion will be discussed, and the method of implementation of this equation in the computational fluid dynamics (CFD) code CFX-TASCflow will be outlined.

3.1 Basic Equations of Turbulence Modeling

Turbulent flows of a viscous, incompressible fluid with constant properties are considered here. The governing field equations are the Navier-Stokes and continuity

equations, which are given by

$$\frac{\partial u_i}{\partial t} + u_j \frac{\partial u_i}{\partial x_j} = -\frac{1}{\rho}\frac{\partial P}{\partial x_i} + \nu \nabla^2 u_i \tag{3.1}$$

and

$$\frac{\partial u_i}{\partial x_i} = 0. \tag{3.2}$$

where u_i is the velocity vector, p is the modified pressure (which can include a gravitational potential) and ν is the kinematic viscosity of the fluid. The Einstein summation convention applies to repeated indices.

Turbulence is random or chaotic in nature. As a result, for practical flows, it is difficult to solve the Navier-Stokes equations exactly for the instantaneous, time-dependent velocities and pressures. It is common practice to use a technique called Reynolds decomposition, where the velocity at a point in space is split into a mean part and a random fluctuating part. The mean (with respect to time) of the fluctuating velocity component is zero. These fluctuating components play an integral role in dispersing particles in the carrier phase.

The time-averaged form of the Navier-Stokes equations can be found by decomposing the velocity and pressure into mean and fluctuating components:

$$u_i = \overline{u_i} + u_i' \quad , \quad p = \overline{p} + p' \tag{3.3}$$

Substituting into the Navier-Stokes equation and time-averaging yields the Reynolds-averaged Navier-Stokes equation, which physically corresponds to a balance of mean

linear momentum. This equation is given below:

$$\frac{\partial \overline{u_i}}{\partial t} + \overline{u_j}\frac{\partial \overline{u_i}}{\partial x_j} = -\frac{1}{\rho}\frac{\partial \overline{p}}{\partial x_i} + \nu\nabla^2\overline{u_i} - \frac{\partial \tau_{ij}}{\partial x_j} \tag{3.4}$$

where:

$$\tau_{ij} = \overline{u_i' u_j'} \tag{3.5}$$

is the Reynolds-tensor. The mean continuity equation is given by

$$\frac{\partial \overline{u_i}}{\partial x_i} = 0 \tag{3.6}$$

and is obtained by simply taking the ensemble mean of the continuity equation. These equations do not represent a closed system for the determination of the mean velocity and mean pressure because of the additional six unknowns contained within the Reynold's stress tensor $(\overline{u'u'}, \overline{v'v'}, \overline{w'w'}, \overline{u'v'}, \overline{u'w'}, \overline{v'w'})$. These terms are called the Reynolds stresses.

The solution of the Reynold's stress tensor is known as the turbulence closure problem. Researchers have come up with many models over the years to solve this problem. The models that are used most often in industry are the $k-\epsilon$ and second-order closure models. These will be described in detail in the next section.

3.2 Turbulence Closure Models

The choice of turbulence model is often a compromise based on the user's desire for accuracy and willingness to take on computational effort. Two-equation models and second-order closure models are two of the most popular methods in industry

for solving the Reynolds-stress closure problem. The $k-\epsilon$ model, a popular two-equation model, has been shown to generate reliable fluid flow predictions for a variety of different flows. The model is considered to have a low computational cost, since it only needs to solve two equations of turbulence quantities to satisfy the closure problem. The second-order closure models solves equations for the Reynolds stresses directly (6 equations),as well as an equation for the dissipation rate, ϵ. This makes it more computationally expensive, but it is considered to be more reliable and robust for a wider range of flows. The two models will be described in more detail in the following sections.

3.2.1 $k-\epsilon$ Model

The $k-\epsilon$ model is among the most popular turbulence models used in scientific and engineering calculations. It is based on an isotropic eddy viscosity model. Two separate modeled transport equations are solved for the turbulent length and time scales. The length and time scales are built up from the turbulent kinetic energy and dissipation rates as follows (Launder & Spalding,1974):

$$l_0 \propto \frac{k^{1.5}}{\epsilon}\ ,\ \tau_0 \propto \frac{k}{\epsilon} \tag{3.7}$$

The $k-\epsilon$ turbulence model provides these variables by solving separate modelled transport equations for the turbulent kinetic energy k and turbulent dissipation rate ϵ (Launder & Spalding,1974). At high Reynolds numbers, the turbulent kinetic energy transport equation is given by:

$$\frac{Dk}{Dt} = \frac{1}{\rho}\frac{\partial}{\partial x_k}\left[\frac{\mu_t}{\sigma_k}\frac{\partial k}{\partial x_k}\right] + \frac{\mu_t}{\rho}\left(\frac{\partial U_i}{\partial x_k} + \frac{\partial U_k}{\partial x_i}\right)\frac{\partial U_i}{\partial x_k} - \epsilon$$

and the transport equation for ϵ is given by:

$$\frac{D\epsilon}{Dt} = \frac{1}{\rho}\frac{\partial}{\partial x_k}\left[\frac{\mu_t}{\sigma_\epsilon}\frac{\partial \epsilon}{\partial x_k}\right] + \frac{C_1\mu_t}{\rho}\frac{\epsilon}{k}\left(\frac{\partial U_i}{\partial x_k} + \frac{\partial U_k}{\partial x_i}\right)\frac{\partial U_i}{\partial x_k} - C_2\frac{\epsilon^2}{k}$$

The $k-\epsilon$ model utilizes the eddy-viscosity assumption to relate the Reynolds stress and turbulent flux terms to the mean flow variables. These models use the gradient diffusion hypothesis to relate the Reynolds stresses to the mean velocity gradients and the turbulent viscosity:

$$\overline{\rho u_i' u_j'} = -\mu_t\left(\frac{\partial \overline{U_i}}{\partial x_j} + \frac{\partial \overline{U_j}}{\partial x_i}\right) + \frac{2}{3}\rho\delta_{ij}k \tag{3.8}$$

where the eddy viscosity is given by

$$\mu_t = C_\mu \rho \frac{k^2}{\epsilon} \tag{3.9}$$

The $k-\epsilon$ model only requires a few empirical constants in the two transport equations to satisfy the closure condition. The values for the constants as suggested by Launder & Spalding can be found in Table 3.1.

TABLE 3.1: The values of the constants in the $k-\epsilon$ model

C_μ	C_1	C_2	σ_k	σ_ϵ
0.09	1.44	1.92	1.0	1.3

The $k-\epsilon$ model generates very good predictions for pipe flows and other boundary-layer flows. The constants that are used in the model have been specifically tuned for these kinds of problems. However, the model tends to have difficulty with more complicated flows that contain effects such as swirl, and especially when curvilinear problems arise (AEA,2001). This is due to the inherent assumption of a scaler turbulent viscosity in the model.

3.2.2 Second Order Closure Models

Although two-equation models are the most commonly used turbulence models, they still have significant deficiencies that make their application to complex turbulent flows precarious. As mentioned earlier, the two-equation models of the eddy-viscosity have the following major deficiencies: (a) the inability to properly account for the streamline curvature, rotational strains, and other body-force effects; and (b) the neglect of nonlocal and history effects on the Reynolds-stress anisotropies. Most of these deficiencies are intimately tied to the assumption that there is a clear-cut separation of scales at the second-moment level (i.e. the level of the Reynolds-stress tensor). While some of the deficiencies cited above can be partially overcome by the use of two-equation models with a nonlinear algebraic correction to the eddy viscosity, major improvements can only be achieved by higher order closures- the simplest of which are second-order closure models (Speziale, 1991).

Second-order closure models are based on the Reynolds-stress transport equation. Since this equation automatically accounts for the convection and diffusion of Reynolds stresses, second-order closure models (unlike eddy-viscosity models) are able to account for strong nonlocal and history effects. Furthermore, since the Reynolds-stress transport equation contains convection and production terms that adjust themselves automatically in turbulent flows with streamline curvature or a system rotation (through the addition of scale factors or Coriolis terms), complex turbulent flows involving these effects are usually better described (AEA,2001).

3.3 Numerical Solution of Fluid Phase

The numerical simulations in this thesis were carried out using the computational fluid dynamics software package CFX-TASCflow. CFX-TASCflow uses a finite volume

method to solve the Navier-Stokes equations. The finite volume method integrates the equations over a fixed control volume, using Gauss's theorem. The integrated form of the Navier-Stokes equations is given as:

$$\frac{\partial}{\partial t}\int_v \rho u_i d_v + \int_s \rho u_j u_i dn_j = -\int_s P dn_i + \int_s \mu_{eff}\left(\frac{\partial \Phi}{\partial x_j} + \frac{\partial u_j}{\partial x_i}\right) dn_j + \int_v S_{u_i} dv \quad (3.10)$$

$$\frac{\partial}{\partial t}\int_v \rho dv + \int_s \rho u_j dn_j = 0 \quad (3.11)$$

where v and s are volume and surface integrals, respectively, and dn_i are the differential Cartesian components of the outward normal surface vector. The effective viscosity, μ_{eff} is the sum of the dynamic and eddy viscosities of the fluid.

The key feature of the finite volume method is the definition of the control volume. The method retains the geometric flexibility of the finite element method while adding the conservation properties of the finite volume method (AEA,2001). The computational domain is discretized into elements, such that each computational node has a representative control volume (see figure 3.1).

The benefit of this method is that the fluxes are evaluated at integration points, which are shared by adjacent control volumes exactly (AEA,2001). Since the same flux that leaves a control volume enters the adjacent control volume, numerical conservation is guaranteed (see figure 3.2).

CFX-TASCflow utilizes a multi-grid solver to solve the resultant algebraic equations. More details on the numerical solver methods of the CFX-TASCflow code can be obtained in the CFX-TASCflow theory manual.

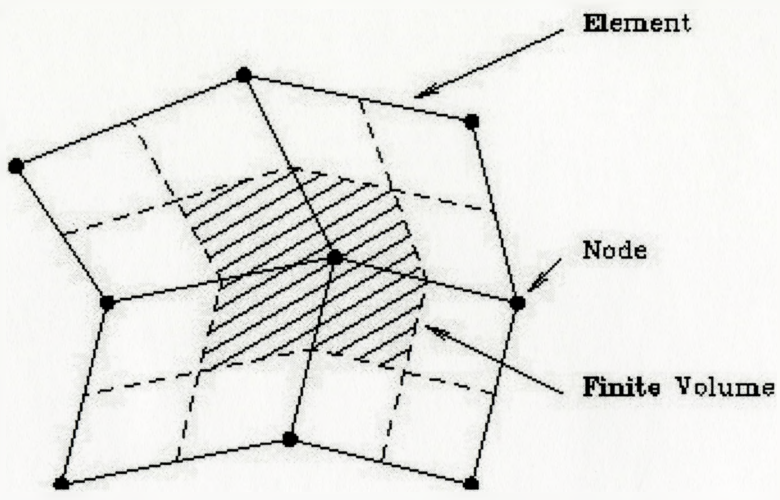

FIGURE 3.1: The definition of the control volume (AEA,2001)

3.4 Numerical Solution of the Particle Equation of Motion

The forces that act on a particle during its motion through a fluid field are due to the difference in velocity between the particle and the local fluid, and the displacement of the fluid by the particle. An equation of motion of the form $F = \sum ma$ can be derived for a particle that takes into account all of the forces that act on the particle due to physical phenomenon such as drag and lift. The particle momentum equation was first derived by Basset (1888), Boussinesq (1903) and Oseen (1927), as was shown in section 2.1.

At low loading ratios, such as in the experiments examined in this thesis, the particles do not influence the gaseous field, and there is therefore no turbulence modulation. The particles are of the small type, and therefore effects such as lift and coriolis forces can be shown to scale out of the problem, and an equation of motion that is solely a

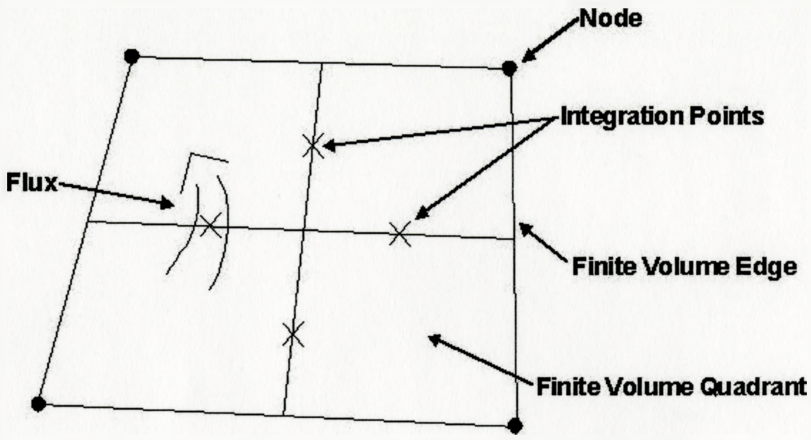

FIGURE 3.2: Integration point definition for a 2-D quadrilateral element (AEA,2001)

function of drag and gravitational forces can be derived for the particles.

$$\frac{du_p}{dt} = \frac{f}{\tau_p}(u_g - u_p) + g \tag{3.12}$$

where

$$f = 1 + 0.15 Re_p^{0.687} \tag{3.13}$$

and

$$\tau_p = \frac{\rho_p d_p^2}{18\mu} \tag{3.14}$$

where u_p and u_g are the instantaneous particle and gas-phase velocities, respectively, τ_p is the particle relaxation time constant, g is acceleration due to gravity, ρ_p is the particle material density, and μ is the fluid viscosity. Equation (3.12) is valid for the range $Re_p < 700$ (Fan & Zhu,1998). Particle trajectories are calculated based on the solution of this equation.

The tracking model implemented in CFX-TASCflow makes some key limiting assumptions. First, it is assumed that the particles do not interact with each other. Particles are injected and tracked one at a time. This limits the use of CFX-TASCflow

to simulations where the mass loading ratio is small (approximately less than 0.1). The mass loading ratio determines the magnitude of the concentration of particles in the simulations, and does not feedback or modulate the turbulence through the momentum equations. Secondly, there are no particle source terms to the turbulence equations, and therefore, turbulence is not modulated by the discrete phase. Finally, the particles are assumed to be spherical and inert (AEA,2001).

3.5 Implementation of Lagrangian Tracking in CFX-TASCflow

Particle displacement is calculated using forward Euler integration of the particle velocity over the computational time step, δt. It should be noted that the computational time step discussed in this section is a sub-time step over which the ordinary differential equation for the particle equation of motion is solved, and not the physical δt over which $u_g^{'}$ is held constant in the correlated particle models discussed earlier. The solution of the Euler integration yields:

$$x_i^n = x_i^o + \left.\frac{dx_i}{dt}\right|_0 \delta t \tag{3.15}$$

where the superscripts n and o refers to the new and old values respectively, and the particle velocity is given by $u_{p,i} = \frac{dx}{dt}$.

In forward integration, the particle velocity calculated at the start of δt prevails over the entire computational time step. At the end of this time step, a new particle velocity is calculated from the solution of the particle equation of motion. While the exact analytical solution of this equation is not trivial, it can be solved analytically as a linear equation if the time step is small enough that τ remains constant

during the integration interval. The integration of the particle equation is given by (Coimbra *et al.*,1998):

$$\nu_p = \nu_f + (\nu_p^o - \nu_f) exp\left(-\frac{\delta t}{\tau}\right) + g\tau\left[1 - \exp\left(-\frac{\delta t}{\tau}\right)\right] \tag{3.16}$$

where

$$\tau = \frac{m_p}{3\pi d_p \mu_f} \frac{1}{(1 + 0.15 Re_p^{0.687})} \tag{3.17}$$

The procedure for determining a particle trajectory through a flux element will be described with the aid of figure 3.3.

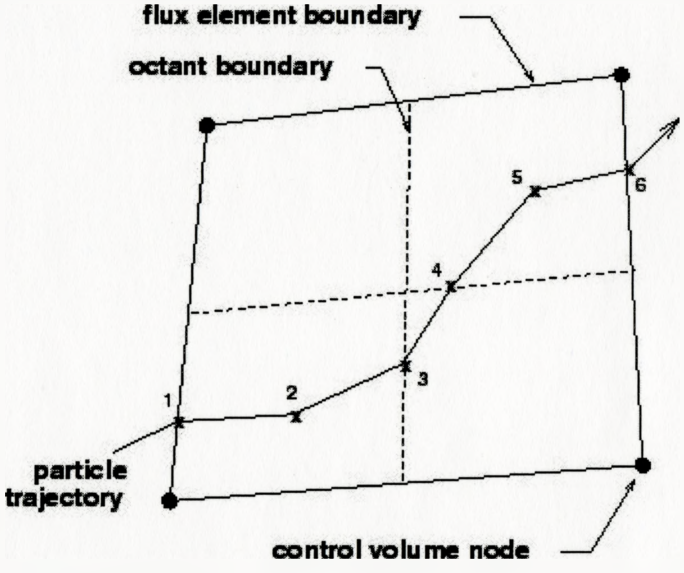

FIGURE 3.3: The definition of the control volume (AEA,2001)

A two-dimensional flux element is shown for clarity. The particle will enter the flux element at point 1 and move to point 2 in one time step. It will then move to point 3 in a second time step. There are three rules which control the tracking of the particle (AEA,2001).

1. A particle cannot travel through any flux element during a time step.

2. A particle may only travel some user-defined fraction of the control volume step per time step.

3. For turbulent particle tracking, the time step is also limited by the lifetime of the eddy or the time required for the particle to cross the eddy.

3.6 Summary

This chapter began with a description of the basic equations of turbulence modelling. The Navier-Stokes and continuity equations were presented in their differential form. The method of decomposition was described and the Reynolds-averaged form of the Navier-Stokes equations was given. As a result, the Reynolds stress tensor was defined and the turbulence closure problem was introduced.

The closure problem was then discussed in some more detail. Two of the more prevalent methods of solution for this problem were introduced: the $k-\epsilon$ and second-order closure models. The $k-\epsilon$ model solves the closure problem by modelling transport equations for the turbulent kinetic energy and dissipation rates based on an eddy-viscosity assumption, and calculating length and time scales based on these results. Second-order models solve the closure model by modelling transport equations for the normal and shear stresses directly. This model is able to solve for curvilinear problems.

The numerical solution of the fluid phase was described in the next section. The CFD code CFX-TASCflow utilizes a finite-volume solution method which integrates the Navier-Stokes and continuity equations over a fixed control volume. This method utilizes the flexibility of a finite element method while ensuring numerical continuity by evaluating fluxes at integration points which are shared by adjacent control

volumes exactly. A multi-grid solver is used to solve the resultant algebraic equations.

Finally, the derivation of the particle equation of motion was outlined. For the flows of interest in this work, the equation of motion of reduces to a function of drag forces and gravity only. The calculation of new particle velocities and implementation of Lagrangian tracking in CFX-TASCflow was also described.

CHAPTER 4

Stochastic Separated Flow Models

Stochastic separated flow (SSF) models use a Lagrangian framework to solve the trajectory equations of a particle as it interacts with a succession of discrete turbulent eddies. First developed by Dukowicz (Gosman & Ioannides,1983), this Lagrangian framework treats the particles as distinct entities within the fluid phase. The solution is stochastic since the particle interacts with the instantaneous velocities of the gas-phase turbulence. The model incorporates the turbulent fluctuations by random sampling to determine the instantaneous velocity of the continuum gas-phase. More precisely, turbulent velocity fluctuations are determined from statistical correlations of such fluctuations.

There are two main distinct groups of SSF models, discrete eddy models and correlated models. The characteristics of these models will be outlined in detail in this chapter, and examples of models of these types will be described.

4.1 Discrete Eddy Models

Discrete eddy models are the simplest of the SSF models. They model the fluid as a collection of discrete eddies, each with a uniform velocity and finite life-time. The particles will then enter eddies, and be subjected to the local eddy velocity for the duration of the eddy-particle interaction. The interaction time is governed by

either the time required for the particle to cross the eddy, or the lifetime of the eddy - depending on whether the crossing-trajectory effect or eddy capture dominates. Gosman & Ioannides (1983) is an example of a discrete eddy model.

4.1.1 The Model of Gosman and Ioannides

In the model of Gosman & Ioannides (1983) the effect of the turbulence on the particle motion is simulated by a stochastic approach. One element of this is the evaluation of the instantaneous gas velocity u from the time-averaged gas velocity U and turbulence energy k fields. This instantaneous velocity is required to evaluate the drag term in the particle equation of motion. For this purpose, the turbulence is assumed to be isotropic and to possess a Gaussian probability distribution in the fluctuating velocity, whose standard deviation σ_{ii} is given by

$$\sigma_{ii} = \frac{2}{3}k^{0.5} = \sqrt{\overline{u_i^2}} \tag{4.1}$$

Random sampling of this distribution at appropriate points in the trajectory calculation then yields the estimated prevailing fluctuating velocity field u' and hence the instantaneous velocity field $u = U + u'$.

A second important element is the manner of determining the time interval t_{int} over which the particle interacts with the randomly sampled velocity field. Here, it is convenient to envisage the latter as being associated with a turbulent eddy, in which case the interaction time is determined by one or the other of the following possible events: 1) the particle velocity is sufficiently close to the gas velocity to allow the particle to remain within the eddy during the whole of the eddy lifetime t_e or 2) the relative or 'slip' velocity between the gas and the particle is large enough to allow the particle to traverse the eddy in a transit time t_{tr} shorter then t_e. The interaction time scale will therefore be the minimum of the above, i.e. $t_{int} = min(t_e, t_{tr})$.

Estimates of the eddy and transit time scales are made under the further assumption that the characteristic size of the randomly sampled eddy is the dissipation length scale l_e, given by

$$l_e = C_\mu^{0.5} \frac{k^{1.5}}{\epsilon} \tag{4.2}$$

The eddy lifetime is then estimated as

$$t_e = \frac{l_e}{|u_g'|} \tag{4.3}$$

where u_g' is the gas-phase velocity fluctuation. The equation that is used to determine the transit time of a particle is given by:

$$t_{tr} = \tau_p \ln \left[1 - \frac{l_e}{\tau_p |\overline{u_f} - \overline{u_p}|} \right]$$

where τ_p is the particle relaxation number. The Lagrangian particle equation of motion is solved repeatedly with u_g' held constant over this interaction interval to generate the trajectory of a particle. The above procedure may be repeated for as many interaction times as are required for a particle to traverse the required distance. In this model (and indeed all SSF models), care must be taken to ensure that a statistically significant number of particle trajectories are calculated. (Gosman & Ioannides,1983).

4.1.2 The Model of Shuen, Chen and Faeth

The model of Shuen, Chen and Faeth (SCF) largely resembles the model of Gosman and Ionnides (GI). It is the default particle dispersion model used in the commercial

CFD code CFX-TASCflow, and will be one of the models tested throughout this work. Shuen *et al.* (1983) proposed modifications to the expressions for characteristic eddy size and the eddy lifetime presented in the GI model. Since the turbulent kinetic energy is related to the fluctuating turbulent velocity component, they defined the eddy lifetime as:

$$t_e = \frac{l_e}{\sqrt{\frac{2}{3}k}} \tag{4.4}$$

In addition, the characteristic eddy size is defined similarly to that of GI, but a different exponent is used, that is $C_\mu^{0.75}$. However, the value of the power that C_μ is raised to is not agreed on by all researchers. Analytical work by Lightstone & Raithby (1998) indicated an exponent of 0.63.

4.2 Correlated Models

Using the Gosman and Ionnides methodology, the turbulent gas-phase velocity fluctuations in each orthogonal direction is sampled only once per eddy and the gas-phase velocity is held constant over the particle/eddy interaction time. With this approach, the particle interaction time is chosen to be large, such that the time correlation between fluctuating velocities in subsequent time steps will be effectively zero. Correlated models build on discrete eddy models, but instead of a series of discrete eddies, the fluid is viewed as a continuum of correlated velocities. The level of correlation can depend upon the size of the time step taken and the distance between points.

4.2.1 Zhou and Leschziner's Time-Correlated Isotropic Model

Zhou & Leschziner (1991a) were the first researchers to present a model based on the hypothesis that there is a temporal correlation between velocity fluctuations at two successive time steps. They introduced a method that used a time-correlation coefficient $R(\delta t)$ defined as:

$$R(\delta t) = \frac{\overline{u_t u_{t-\delta t}}}{\overline{u^2_{t-\delta t}}}$$

which they approximated, based on a suggestion by Hinze (1975), as:

$$R(\delta t) = \exp\left(\frac{-\delta t}{T}\right)$$

where $T = \gamma(C_\mu^{0.75} k^{1.5}/\epsilon)(2/3k)^{0.5}$. The value of the empirical constant γ was taken as 0.8 based on an optimization carried out by Zhou & Leschziner for isotropic turbulence. As a result, it was possible to sample velocity fluctuations that were correlated in time using the equation:

$$u'_t = R(\delta t) u'_{t-\delta t} + e_t \tag{4.5}$$

where e_t is an independent random variable that approximates all the effects of randomness during a time step δt. The variance of e_t can be determined by re-writing equation (4.5), squaring both sides of the equation, and taking the expected value.

$$\overline{e_t^2} = \overline{(u'_t - R(\delta t) u'_{t-\delta t})^2} = \overline{u'^2_t} - R^2(\delta t)\overline{u'^2_{t-\delta t}}$$

The model of Zhou & Leschziner allows particles to be exposed to more then one instantaneous velocity during the interaction period with the eddy, which closely

models the physics of the flow. However, the model does not account for the crossing trajectory effect (CTE), which describes the movement of a particle from one eddy to another due to a difference in velocities between the particle and the fluid. This phenomenon has been shown to significantly affect the dispersion of particles (Csanady,1963). Zhou & Leschziner's model assumes that the fluid trajectories and particle trajectories are very close, which is only true for particles with small relaxation times.

4.2.2 Hennick and Lightstone's SSF Model

Hennick & Lightstone (2000) developed a model built on Zhou and Leschziner's time-correlated, isotropic, stochastic model. This model accounts for time-correlation by considering a particle to be exposed to many correlated fluctuating velocities during its interaction period with an eddy. The crossing trajectory effect is incorporated by introducing a spatial correlation coefficient based on the relative velocity of the particle and the time step δt. The spatial auto-correlation was derived based on work by Lu, Fontaine, and Aubertin. In addition, the magnitude of the Lagrangian integral time scale is determined independent of the model's performance by relating the variance of particle position to Taylor's result for fluid particles.

Incorporating the approximations for the temporal and spatial autocorrelation, the gas-phase velocity fluctuation becomes:

$$u_i' = R(\delta t)R(\delta x)u_{t-\delta t}' + e_t \tag{4.6}$$

where the temporal autocorrelation is the same as in the time-correlated isotropic

model of Zhou & Leschziner and the spatial autocorrelation is approximated by

$$R(\delta x) = \exp\left(-\frac{u_{REL}\delta t}{L_I}\right) \tag{4.7}$$

where the Lagrangian integral timescale is given by $\tau_{LI} = 0.135k/\epsilon$, $u_{REL} = |u_g - u_p|$ and L_I is the Lagrangian integral length scale given by:

$$L_I = C_\mu^{0.63}\frac{k^{1.5}}{\epsilon} = 2\tau_{LI}\sqrt{\frac{2}{3}k} \tag{4.8}$$

Similar to the model of Zhou & Leschziner, the expected value of e_t is zero, although the variance has a slightly different form given by

$$\overline{e_t^2} = \overline{u_t'^2} - R^2(\delta t)R^2(\delta x)\overline{u_{t-\delta t}'^2} \tag{4.9}$$

This model is isotropic in nature, and as such does not take into account the anisotropy of turbulent shear flows.

4.2.3 Zhou & Leschziner's Anisotropic Model

Zhou & Leschziner (1991b)'s anisotropic model is an improvement of their earlier correlated model because of it's ability to account for anisotropy and correlation between velocity fluctuations. However, as noted by the authors, the model does not account for the crossing trajectory effect.

The model allows for anisotropy by making the new velocity fluctuations in any different direction a function of the velocity fluctuations in all directions, as opposed to the isotropic form of equation (4.5).

$$u_t = \beta_{xx}u_o + \beta_{xy}v_o + \beta_{xz}w_o + d_{tx} \tag{4.10}$$

$$v_t = \beta_{yx} u_o + \beta_{yy} v_o + \beta_{yz} w_o + d_{ty} \tag{4.11}$$

$$w_t = \beta_{zx} u_o + \beta_{zy} v_o + \beta_{zz} w_o + d_{tz} \tag{4.12}$$

where u_o, v_o and w_o are the old velocities and u_t, v_t and w_t are the new velocities. To solve this set of equations, it is necessary to find expressions for the β's and the d's.

By multiplying equation (4.10) by u_o and time averaging, a new equation is generated:

$$\overline{u_t u_o} = \beta_{xx} \overline{u_o u_o} + \beta_{xy} \overline{v_o u_o} + \beta_{xz} \overline{w_o u_o} \tag{4.13}$$

Similarly, equation (4.10) can be multiplied by v_o and w_o and time-averaged to yield two more equations:

$$\overline{u_t v_o} = \beta_{xx} \overline{u_o v_o} + \beta_{xy} \overline{v_o v_o} + \beta_{xz} \overline{w_o v_o} \tag{4.14}$$

$$\overline{u_t w_o} = \beta_{xx} \overline{u_o w_o} + \beta_{xy} \overline{v_o w_o} + \beta_{xz} \overline{w_o w_o} \tag{4.15}$$

To fully understand the previous step, it is important to note that the term $\overline{d_{tx} u_o} = 0$, since the terms d_{tx} and u_o are independent variables. Six more equations can be generated in a similar manner by multiplying equations (4.11) and (4.12) by the three velocity components and time-averaging. The three sets of equations can then each be written in matrix form:

$$[R]\overline{\beta} = \overline{C} \tag{4.16}$$

It is then simple to solve for the β terms simply by multiplying both sides of the equation by the inverse of the Reynolds stress matrix:

$$\overline{\beta} = [R]^{-1}\overline{C} \tag{4.17}$$

The methodology of obtaining the statistical properties of the d's in Equations (4.10) to (4.12) is a little more involved than the solution for the β's.

To make sure that the d's have the correct statistical behavior, information is needed for: $\overline{d_{tx}^2}$,$\overline{d_{ty}^2}$ etc. This information can be obtained by manipulating the equation:

$$u_t = (\beta_{xi} u_{io}) + d_{tx} \tag{4.18}$$

Squaring both sides of each equation gives us the variance, noting that $\overline{d_{tx} u_{io}} = 0$ gives:

$$\overline{u_t^2} = \overline{(\beta_{xi} u_{io})^2} + \overline{d_{tx}^2} \tag{4.19}$$

It is then simple to see that:

$$\overline{d_{tx}^2} = \overline{u_t^2} - \overline{(\beta_{xi} u_{io})^2} \tag{4.20}$$

Similarly,

$$\overline{d_{ty}^2} = \overline{v_t^2} - \overline{(\beta_{yi} u_{io})^2} \tag{4.21}$$

$$\overline{d_{tz}^2} = \overline{w_t^2} - \overline{(\beta_{zi} u_{io})^2} \tag{4.22}$$

Now that all of the statistical data on the d's has been obtained, it is just necessary to generate the terms. For this purpose, Zhou & Leschziner used the following forms:

$$d_{tx} = b_{11} z_1 \tag{4.23}$$

$$d_{ty} = b_{21} z_1 + b_{22} z_2 \tag{4.24}$$

$$d_{tz} = b_{31} z_1 + b_{32} z_2 + b_{33} z_3 \tag{4.25}$$

where z_1, z_2 and z_3 are a set of random variables with independent standard normal distribution $N(0,1)$. The b's are then solved for with the aid of the statistical properties of the d's, i.e.

$$\overline{d_{tx}^2} = b_{11}^2 \overline{z_1^2} = b_{11}^2 \tag{4.26}$$

Therefore, it is simple to see that

$$b_{11} = \sqrt{\overline{d_{tx}^2}} \tag{4.27}$$

The remaining b's can be solved for by similar back-substitution. Now that the mechanics of the anisotropic, correlated model have been described in detail, it will be instructive to detail the correlation function that the authors favored. The velocity fluctuation is described by Zhou & Leschziner using a time-correlation coefficient derived for fluid particles:

$$R_{ij} = \frac{\overline{u_i u_j}}{\sqrt{\overline{u_i^2}}\sqrt{\overline{u_j^2}}} \exp\left[-\frac{\delta t}{T_{ij}}\right] \cos\left[\frac{\delta t}{T_{ij}}\right] \tag{4.28}$$

where T_{ij} is a time scale given by:

$$T_{ij} = \beta(C_\mu^{0.75} k^{1.5}/\epsilon)/(\sqrt{\overline{u_i^2}}\sqrt{\overline{u_j^2}})^{0.5} \tag{4.29}$$

The value of β was taken as 0.8 on the basis of an optimization carried out by the authors. The correlation utilizes a 'Frenkiel-type' form whose usage is not recommended in work completed by Lightstone (2001) since it produces a correlation that differs from the original intended correlation. As well, unless a particle has a small particle relaxation time, it will not be able to follow the high-frequency fluctuations of the turbulence, and in general, will not see the same velocity fluctuations as a fluid point. Thus, a particle falling through an eddy will see a velocity fluctuation at time t that should have a much lower correlation. Using Zhou and Leschziner's model, however, a heavy particle sees velocity fluctuations that are highly correlated. Hence, the model is unable to capture the crossing trajectory effect.

4.2.4 Berlemont's Model

The model of Berlemont *et al.* (1990) is very similar to Zhou and Leschziner's anisotropic model for dispersion, except the authors have included a Eulerian spatial correlation to account for the crossing trajectory effect of particles. If the discrete particle and the fluid particle are moving too far away from each other (i.e. relative velocities are large), the instantaneous fluid velocity 'encountered' by the discrete particles cannot be estimated by the scheme. Berlemont defines a length scale L_D which characterizes the correlation domain. When the discrete particle is outside the domain, i.e. when $r > L_D$, Berlemont 'changes' the fluid particle. The trajectory of the new fluid particle is then simulated from the location of the discrete particle. The whole process leads to a discrete particle trajectory Lagrangian simulation, and theoretically solves the problem (Berlemont *et al.*,1998).

Berlemont expresses the Lagrangian correlation as follows:

$$R_{ij} = \exp\left[\frac{-\delta t}{(m^2+1)\tau_L}\right]\cos\left[\frac{m\delta t}{(m^2+1)\tau_L}\right] \tag{4.30}$$

In this equation, τ_L is the Lagrangian integral time scale and m is a parameter which determines the number of negative loops in the correlation function and is therefore linked to the type of flow under consideration. For the simple case of homogeneous isotropic turbulence $m = 0$ can be used, which gives the correlation function an exponential form without negative values (Burry & Bergeles,1993).

For $m = 0$, the equation becomes:

$$R_{ij} = \exp\left[\frac{-\delta t}{\tau_L}\right] \tag{4.31}$$

and for $m = 1$:

$$R_{ij} = \exp\left[\frac{-\delta t}{2\tau_L}\right]\cos\left[\frac{\delta t}{2\tau_L}\right] \tag{4.32}$$

Berlemont proposes using a Frenkiel family of spatial correlations similar to:

$$u_i u_j = \sqrt{\overline{u_i^2 u_j^2}}\exp\left[\frac{-r}{(m^2+1)L_{Eij}}\right]\cos\left[\frac{mr}{(m^2+1)L_{Eij}}\right] \tag{4.33}$$

where $r = U_{REL}\delta t$.

So, for $m = 0$, this model becomes:

$$u_i u_j = \sqrt{\overline{u_i^2 u_j^2}}\exp\left[\frac{-r}{L_{Eij}}\right]$$

and for $m = 1$, the model becomes:

$$u_i u_j = \sqrt{\overline{u_i^2}\,\overline{u_j^2}} \exp\left[\frac{-r}{2L_{Eij}}\right] \cos\left[\frac{r}{2L_{Eij}}\right] \tag{4.34}$$

Berlemont *et al.* suggests that ideally the anisotropic length scales L_{Eij} should be calculated from experimental data whenever possible. Otherwise, they suggest using the following forms:

$$\tau_{Lij} = C_L \frac{\overline{u_i u_j}}{\epsilon} \tag{4.35}$$

and

$$L_{Eij} = C_{ij} \sqrt{\overline{u_i u_j}}\, \tau_{Lij} \tag{4.36}$$

where C_{ij} is a constant depending on the scale considered. For isotropic turbulence, $L_{E22} = L_{E11}/2$, when L_{E11} is known, for instance. The constant C_L is taken equal to 0.2 for jets or pipe flows. The correlation length scale L_D is taken as an arithmetic mean value between the normal scales.

While this model has incorporated a Eulerian spatial correlation to account for the crossing trajectory effect, the use of a Frenkiel correlation with a loop parameter results in an inconsistency between the calculated fluid velocity correlation and the original intended correlation, as shown in the paper of Lightstone (2001), and is therefore undesirable.

4.2.5 Burry and Bergeles' Model

Burry & Bergeles (1993) utilize similar Frenkiel functions as Berlemont for calculating the correlations $\overline{u_i u_j}$. The correlation scales are defined differently from Berlemont, to

account for the event of negative Reynolds shear stresses that would lead to physically impossible negative values of the Lagrangian cross-time scales.

$$L_{Eij} = C_{ij}\tau_{Lij}\sqrt{\frac{\overline{u_i^2} + \overline{u_j^2}}{2}} \quad , \quad \tau_{Lij} = C_L\frac{\overline{u_i^2} + \overline{u_j^2}}{2\epsilon} \tag{4.37}$$

where C_L is taken to be 0.2 for jets or pipe flows, ϵ is the turbulent energy's rate of dissipation and C_{ij} are constants depending on the scale and the turbulence field. In their paper, Burry & Bergeles take C_{ij} to be unity for their calculations.

4.3 Evinou & Lightstone Model

The Evinou & Lightstone model is a hybrid of the Burry and Bergeles model and the Hennick and Lightstone model. The intent is to have an anisotropic correlated model that does not use Frenkiel functions, and takes into account the 'crossing trajectory effect'. The form of the correlation functions will be:

$$u_{ip}u_{jf} = \sqrt{\overline{u_{ip}^2}\overline{u_{jf}^2}}exp\left(-\delta t\left(\frac{1}{\tau_{ij}} + \frac{U_{REL}}{L_{Eij}}\right)\right) \tag{4.38}$$

This is consistent with Berlemont's model, with $m = 0$. The value of τ_{ij} will be consistent with the Hennick and Lightstone model, which was derived analytically using Taylor's Theorem for homogeneous isotropic turbulence and given by $\tau_{LI} = 0.135k/\epsilon$. The scales for the spatial autocorrelation will be defined similarly to Burry & Bergeles:

$$L_{Eij} = C_{ij}\tau_{Lij}\sqrt{\frac{\overline{u_i^2} + \overline{u_j^2}}{2}} \quad , \quad \tau_{Lij} = C_L\frac{\overline{u_i^2} + \overline{u_j^2}}{2\epsilon} \tag{4.39}$$

4.4 Summary

In this chapter, the group of Lagrangian particle dispersion models known as the stochastic separated flow models were introduced. The models generate velocity fluctuations through use of random sampling of a variable that is derived from the flow properties of the turbulence. There are two distinct types of stochastic separated flow models: discrete eddy models and correlated models.

Discrete eddy models are characterized by trapping a particle inside an eddy for a finite interaction time. During this interaction time, the particle is exposed to the instantaneous velocity of the eddy for the duration. Two researchers who have contributed models of significance in this category are Gosman & Ioannides (1983) and Shuen *et al.* (1983).

The second type of stochastic separated flow model is the correlated model. These models assume that a particle is exposed to a series of correlated velocities while trapped inside an eddy. The first correlated model to appear in the literature was a time-correlated model proposed by Zhou & Leschziner (1991b). Subsequent work by Berlemont *et al.* (1990) and Burry & Bergeles (1993) have added the complexity of anisotropy and directional correlations.

The chapter was concluded by introducing the proposed model of Evinou and Lightstone. This model is a correlated, anisotropic model similar to that of Zhou & Leschziner (1991b). However, the model incorporates the crossing trajectory through the use of a Lagrangian correlation function similar to that used in the model of Burry & Bergeles (1993). The model incorporates constants in the calculation of the anisotropic length scales that have been derived analytically from Taylor's solution for particle dispersion in homogeneous, isotropic flow.

CHAPTER 5

The Experiment of Lazaro and Lasheras, 1989

The first case that was studied was the dispersion of fine water droplets in a free shear layer which was examined experimentally by Lazaro & Lasheras. This experiment was chosen specifically because the experimenters Zhou & Leschziner used this case to test the performance of their anisotropic, time-correlated stochastic separated flow model, which is the foundation of the model that is proposed in this work. Measurements of particle concentration growth rate and downstream concentration profile were compared to results generated by the models of Shuen *et al.*, Hennick & Lightstone, Zhou & Leschziner and the proposed model of Evinou and Lightstone using the CFX-TASCflow computational fluid dynamics code.

The chapter begins with a description of the experiment. The numerical simulation is described, and the predictions of each model are presented. Results are discussed in detail.

5.1 Description of Experiment

Lazaro & Lasheras constructed a test rig which consisted of an atmospheric pressure, open-return, two dimensional wind tunnel in which a cloud of fine water droplets is

uniformly dispersed into a turbulent air matrix. The uniform-density, one dimensional water spray produced in the tunnel then discharges into a test section. The spray is initially separated from the stagnant air by a splitter plate. At its trailing edge, the spray is allowed to meet and to mix with a stagnant air flow and a two-dimensional turbulent mixing layer is formed.

Velocity moments to third order were obtained in the experiment using flying and stationary hot-wires. The test rig was capable of producing a range of uniform-density water sprays, with the details of the spray used in this work outlined in Table 5.1.

TABLE 5.1: Spray statistics

Quantity	Symbol	Value
Velocity (m/s)	U_0	15
Liquid/air ratio	γ	1.6x10-5
Particle diameter (μm)	d_p	25
Particle density (kg/m^3)	ρ_p	1000

Measurements of the particle concentration field were achieved through simultaneous measurement of laser attenuation and far field diffraction patterns produced by the water droplets as a 3mm diameter laser beam was passed along the homogeneous z coordinate. The distribution of the droplet sizes were then calculated by using Fraunhofer diffraction theory. This information, together with the laser attenuation signal, enabled the particle concentration fields to be measured (Lazaro & Lasheras, 1989).

Estimates of the error in the measurements are given in Table 5.2. These estimations include both the inherent errors of the techniques and the signal-to-noise ratio of the measurements and the statistical errors associated with the finite length of the records (Lazaro & Lasheras,1989). Estimates are given for both gas velocity u_g and particle concentrations, α_p.

TABLE 5.2: Per cent estimated measurement errors for a 95% confidence interval

	Mean	R.m.s.
u_g	±1.5	±4.1
α_p	±4.5	±5.0

There was some concern that the water droplets used in the experiment may deform due to motion relative to the air. Droplet deformation can be characterized by the Weber (We) number, which relates the aerodynamic inertial forces to the surface tension of the liquid phase. It may be written as:

$$We = \frac{\rho V^2 L}{\sigma} \tag{5.1}$$

In the experiment of Lazaro & Lasheras, the Weber number of the particles is quite low due to the small relative velocity between the gas and the particles, as well as the small diameter of the particles. The resultant Weber number is much smaller then the critical value, and deformation of particles can therefore be neglected (Fox & McDonald,1992).

5.2 Description of Boundary Conditions and Simulation

Since the shear layer is two-dimensional in nature, it is possible to model the flow by using a rectangular duct (see Figure 5.1) and applying symmetry boundary conditions in the third direction. The height of the duct was $0.26m$ and the axial length was $1m$. The use of symmetry boundary conditions significantly reduced the complexity of the problem, and thus enabled a much finer mesh to be used in the calculations, since

only three nodes were required to model the ducts depth. Nodes were concentrated on the y axis, where the sharpest gradients were expected. Expansion factors of 3% were used from the centerline of the shear layer in this direction, so that the distance between nodes in the core region of the shear layer is small, and the distance between nodes in the far fields is large. In the axial direction, nodes were again concentrated in the core region of the shear layer, but since smaller gradients were expected, an expansion factor of 1% was used. It was found that a mesh consisting of 140 nodes in the axial direction and 141 nodes in the cross-stream direction was sufficient to generate a grid independent solution.

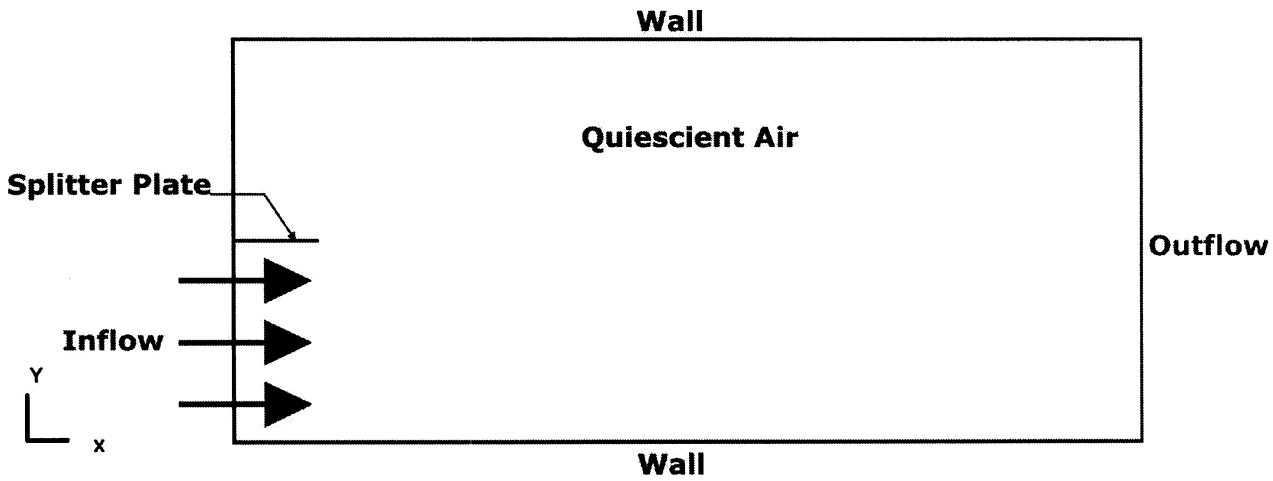

FIGURE 5.1: Geometric representation of model and Boundary Conditions

For the inlet condition, which specifies that the fluid flows across the boundary surface into the solution domain, CFX-TASCflow requires that the velocity, turbulence intensity and energy containing eddy length scale be supplied. Lazaro & Lasheras provided both the inlet velocity profile (see Figure 5.2) and the rms profile at the inlet in their paper. The outlet boundary condition in CFX-TASCflow specifies that the fluid flow across the boundary surface is out of (or exiting) the solution domain. The code requires a static pressure to be evaluated over the entire outlet boundary surface. The wall boundary condition specifies that the fluid cannot flow across the

boundary. The fluid at the wall is assumed to be at rest relative to the wall. The symmetry boundary condition specifies that all gradients are equal to zero at the boundary (i.e. $\frac{\partial \Phi}{\partial z} = 0$), and that there is no flow through it.

The particle boundary conditions are relatively straight-forward. At the inlet, the mass flow rate and velocity of the particles must be specified. This information was available in Lazaro & Lasheras's paper. At the outlet boundary condition, particles 'escape' the solution domain, and are no longer tracked. At the wall boundary a particle, upon impact with the wall, reflects at an angle related to the coefficient of restitution, which determines the component of velocity normal to the surface after impact. In this case, the particles were allowed to reflect 'perfectly' from the wall, or more precisely, at an angle of 90 degrees. Particles are similarly reflected at 90 degrees upon impact with a symmetry boundary condition. More information on the particle tracking techniques incorporated in CFX-TASCflow are available in the code documentation (AEA,2001).

Finally, the correlated models generate velocity flow fluctuations that are correlated in time. As such, the time step, δt, over which velocity fluctuations are held correlated is of great importance. The general idea is that δt should be some fraction of the eddy integral time scale, given by $\tau_{LI} = 0.135 \cdot k/\epsilon$. For this experiment, the average integral time scale in the computational domain was calculated to be approximately $0.001s$. Therefore, a time step of $0.0001s$ was used in the simulations of the experiment, as it was found that this was a significantly small time step to generate particle tracks that were independent of changes in δt.

5.3 Results

Lazaro & Lasheras provided the inlet velocity profile for the flow. It was therefore possible to create a good approximation of the exact inlet conditions of the experiment

(see Figure 5.2) in the simulation. From this figure, it can be seen that the profile matches the experimental data very well.

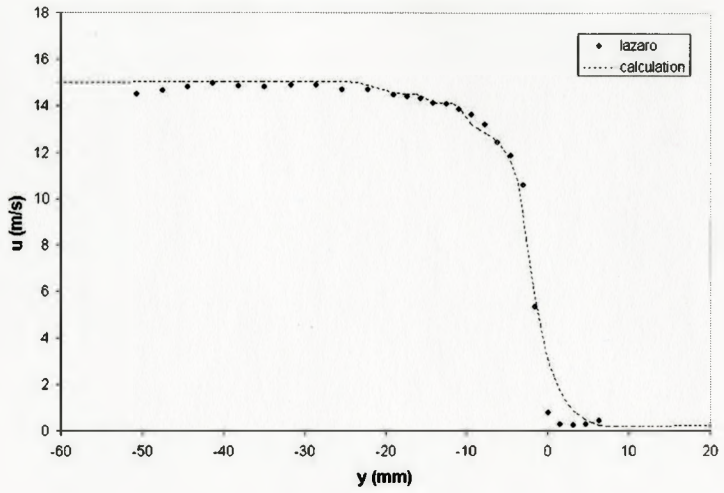

FIGURE 5.2: Longitudinal mean velocity profiles at x=0mm

As well, Lazaro & Lasheras provided the mean particle concentration profile at the inlet (see Figure 5.3). Again, it was possible to model this profile in CFX-TASCflow, although the simulated profile is slightly wavy due to a limitation in the number of particles injected. The waviness of the profile is restricted to the area of the flow removed from the main region of shear however, and it was not anticipated that the particles injected in the 'wavy' region would contribute to the spread of the profile significantly; rather, they would simply be convected axially by the flow. Approximately 70000 particles were injected to generate this profile, which was shown to be insensitive to an increase in particle number in the area of maximum shear. To remove the waviness of the profile would require a number of particles that was deemed to be too computationally expensive for the diminishing benefits.

As a reminder, this experiment was selected because the Zhou & Leschziner used Lazaro & Lasheras's results to assess their anisotropic, time-correlated dispersion

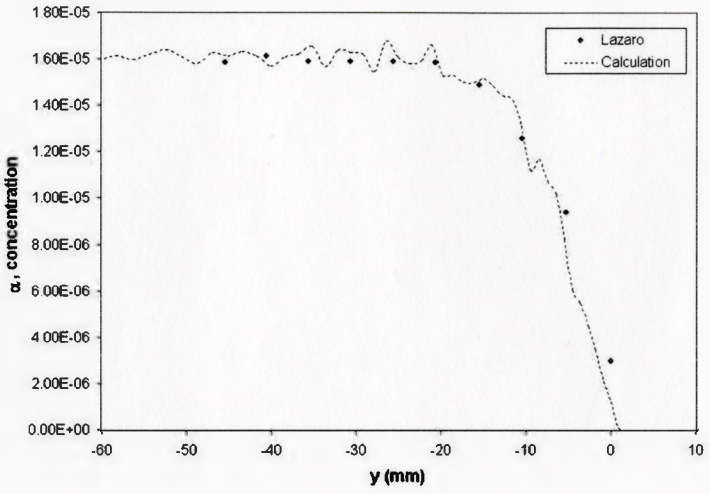

FIGURE 5.3: Mean particle concentration at x=0mm

model. It is possible then to use this case as a validation of the coding of their model, and of the calculation technique. In Figure 5.4 it can be seen that the CFX-TASCflow prediction for spread rate of the fluid mixing layer is underpredicted in comparison to the results generated by Zhou & Leschziner. It should be noted that Zhou & Leschziner used a boundary-layer algorithm incorporating the second-moment closure of Gibson & Launder. This model differs from the second-moment algorithm of Launder, Reece and Rodi, which is incorporated in the CFX-TASCflow code, since it accounts for gravitational effects and the modification of the fluctuating pressure field by the presence of a wall. The Gibson & Launder algorithm was shown to give strong agreement with measurements in a free stratified shear flow of other experimenters (Gibson & Launder,1978). However, since buoyancy issues are not really important in the experiment of Lazaro & Lasheras, it is reasonable to assume that the difference due to choice of closure model is probably insignificant in this case.

The under prediction of the spread rate is more clearly seen in Figure 5.5, which depicts the dimensionless velocity profile at the downstream location $x = 203mm$.

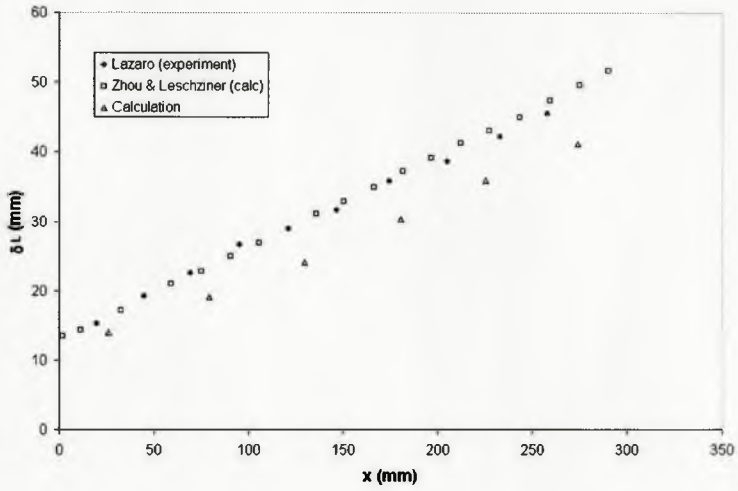

FIGURE 5.4: Aerodynamic spreading rate

The calculated profile has a sharper slope in the transition region, and the points of 10% and 90% velocities are closer together then for the experimental data. This results in a smaller value for the level thickness, which is defined as:

$$\delta_L = y(z = 0.1) - y(z = 0.9) \tag{5.2}$$

or, more precisely, the difference in cross-stream coordinates corresponding to the points where the velocity profile is 10% and 90% of that of the free stream value. The experimenters Zhou & Leschziner made no mention of whether or not their calculated prediction captured the experimental downstream velocity profile correctly.

An under-prediction of aerodynamic spread rate means that the CFX-TASCflow code was unable to correctly predict the streamlines of the shear layer flow. In terms of particle dispersion, this inability should have a profound effect on the dispersion predictions, since particles are convected by the fluid, and therefore follow the streamlines of the flow quite closely. The turbulent fluctuations of the fluid act to disperse particles from the streamlines of the flow; however, when the velocity of the fluid is high,

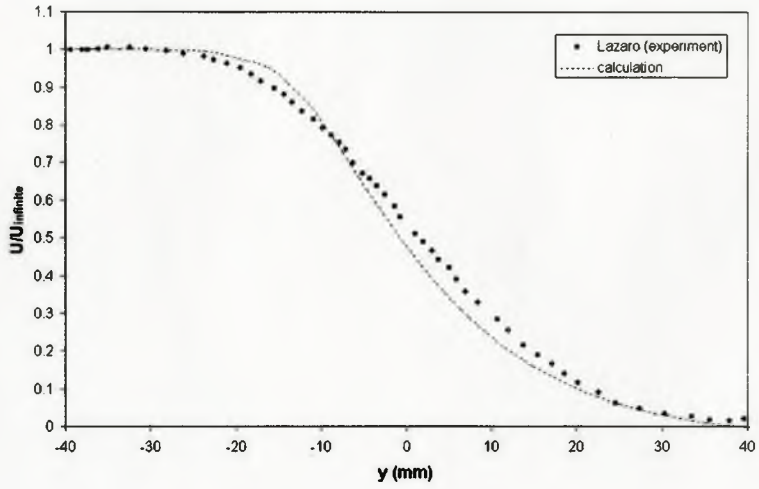

FIGURE 5.5: Dimensionless velocity profile, x=203mm

the particle will be convected very quickly downstream. Thus, if a particle is trapped on an erroneously high velocity streamline, it is reasonable to expect that particles dispersion to be in error by a factor greater then the error in velocity prediction.

As such, when we compare predictions for particle spread rate with axial distance (see Figure 5.6) for the model of Zhou & Leschziner, the predictions generated by the CFX-TASCflow code are in error by as much as 80% from those published by Zhou & Leschziner. It is reasonable to assume that this discrepancy is due to a compounding error effect because of the inaccuracy of the streamline predictions by the CFX-TASCflow code. It is interesting to note that Zhou & Leschziner's data also underpredicted the concentration spreading rate by as much as 20%.

Particle tracking simulations were also carried out using CFX-TASCflow for the dispersion models of Shuen *et al.*, Hennick & Lightstone and the proposed model of Evinou and Lightstone. The predictions of these models (as seen in Figure 5.7) all underpredict the dispersion of the particles for this case. All four models (the Zhou & Leschziner model has been included) generate similar predictions for the particle

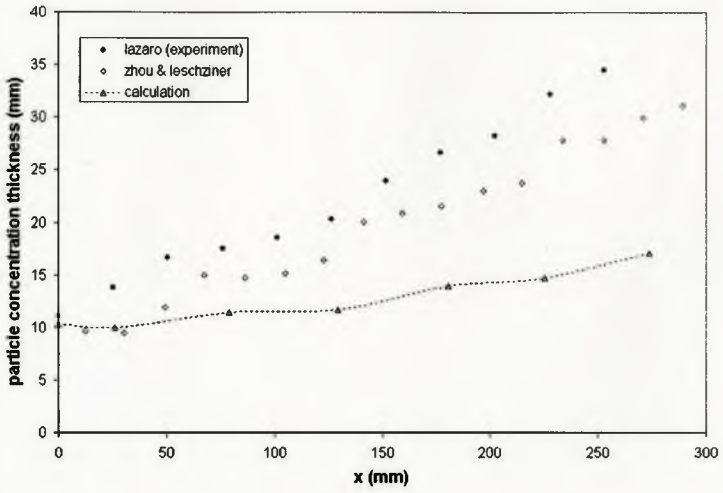

FIGURE 5.6: Comparison of particle spread rate prediction using Zhou and Leschziner's model

spread rate, and it is difficult to say one model is outperforming the others in this case.

Finally, it is instructive to look at the dimensionless particle concentration profile predictions for the four SSF models (see Figure 5.8). It can be seen that the concentration profiles have the same shape as the velocity profile predictions, but have an exaggerated error. It is important to remember that particles are convected by the mean flow, and therefore follow the streamlines of the flow, and are dispersed from these streamlines by the turbulent fluctuations. Since the spread of the streamlines are underpredicted, this has a compound effect on the particle concentration profiles, which are very underpredicted. Another potential reason for the dramatic underprediction may be that the high particle velocity fluctuations that are observed experimentally are usually attributed to particle interactions with large unsteady, vortical structures in the shear layer, which are not modelled by turbulent closure models (Coimbra *et al.*,1998).

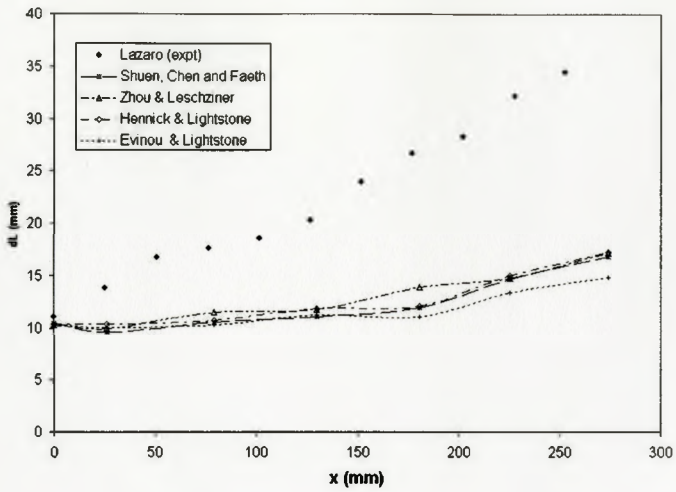

FIGURE 5.7: Comparison of particle spread rate predictions for four SSF models

5.4 Conclusions

This chapter outlined the modelling of the experiment conducted by Lazaro & Lasheras on measurements of the velocity and particle concentration fields across a two-dimensional mixing region formed between a uniform-concentration spray and a stagnant air region. The flow field predictions generated by CFX-TASCflow were compared to the calculations generated by the researchers Zhou & Leschziner for this experiment in an attempt to validate the methodology. It was found that CFX-TASCflow, using the second order closure model of Launder, Reece and Rodi, underpredicted the growth of the mixing layer by as much as 10% at some downstream locations. The particle concentration predictions that were generated using the model of Zhou & Leschziner and CFX-TASCflow were compared to the results presented in their paper, and were shown to be underpredicted. It was surmised that the reason for this under-prediction was a compounding of error due to the inability of the CFX-TASCflow code to accurately predict the streamlines of the shear flow. This process was repeated for the particle dispersion models of Shuen *et al.*, Hennick & Lightstone, and the proposed

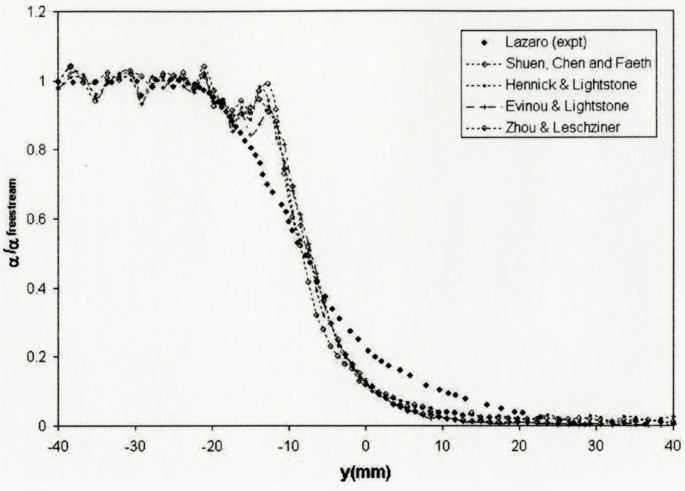

FIGURE 5.8: Comparison of concentration profiles for four SSF models at x=203mm

model of Evinou and Lightstone with similar results.

CHAPTER 6

The Experiment of Yuu et al, 1978

The numerical models described in Chapter 4 were applied and compared with experimental data for the case of a dust laden turbulent round jet. The experimental conditions used in these simulations are the same as those reported in Yuu *et al.* (1978). The experiment was simulated using the CFD code CFX-TASCflow. Measurements of particle concentrations in the axial and radial directions were compared to results generated by each model considered in this thesis.

The chapter begins with a description of the experiment. The numerical simulation is described, and the predictions of each model are presented. Results are discussed in detail.

6.1 Description of Experiment

In this experiment the round jet originates from a nozzle $8mm$ in diameter. The nozzle was designed to produce uniform velocity at the outlet. The resulting round jet exhausted into a large chamber confined between two horizontal walls extending 1.5 m downstream from the nozzle exit and 0.4 m to either side of the center line. The velocity of the gas and the particles at the nozzle inlet was $U_o = 20m/s$. Velocities were measured with a pitot-static probe (2 mm diameter) and Gottingen micromanometer (Yuu *et al.*,1978). Particle concentration measurements were performed using a

photoelectric dust counter. The particles used in the experiment were composed of fly ash because of its spherical shape and low relaxation time. The properties of the particles used in the simulation can be found in Table 6.1.

TABLE 6.1: Particle Properties

Mean Diameter d_p (μm)	Standard Deviation $\sigma(\mu m)$	Density $\rho(g/cm^3)$	Relaxation Time (sec)
15	2.1	2.0	0.014

6.2 Description of Boundary Conditions and Simulation

Since the actual experimental setup dimensions were chosen so as to remove the influence of the boundaries on the formation of the jet, it was possible to only model a subsection of the test section for computational efficiency. As well, due to the axisymmetry of the round jet, only a quarter of the rectangular duct was modelled (see Figure 6.1). The duct was made to be 0.6m long and 0.16m high and wide, which enabled particle predictions to be generated up to a downstream location of $x/D = 70$; the maximum axial location were particle data was reported; and well in excess of $r/x = 0.12$, the maximum radial distance for which data was reported by Yuu *et al.*

The nozzle was modelled as square, with the length of the side of the square being selected so that the area of the square was equivalent to the area of the round nozzle, thus ensuring the same mass flow as in the experiment. This decision was made out of necessity because attempts to model the round jet directly were unsuccessful due to convergence problems. The assumption is that a square jet will closely resemble

the properties of a round jet in the far field. It is allowed that the solution in the near field will most likely be different then in the experimental case, but it is hoped that these differences will have negligible effects on the far field particle concentration profiles.

The boundary conditions used in the simulation can also be seen in Figure 6.1. The inlet was modelled using an inflow condition. Since only one quadrant of the rectangular domain was modelled, symmetry boundary conditions were used on the y and z axes. The rest of the domain was modelled as an opening boundary condition, which allows fluid to flow in and out of the solution domain.

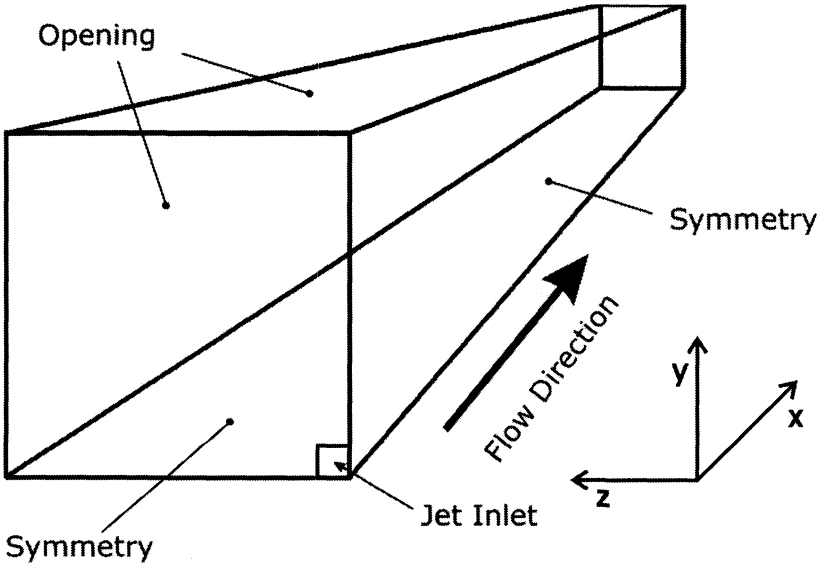

FIGURE 6.1: Geometric representation of model and Boundary Conditions

An important step in numerical simulation is verifying that the obtained solution is independent of the computational grid. In simplest terms, adding or subtracting complexity from the computational grid should not affect the numerical solution in anyway. To verify that the numerical solution was indeed grid independent, simulations were run on two grids of varying refinement: $60X61X61$ and $80X81X81$. The results in Figure 6.2 show that the solution for radial velocity profile at two

downstream locations from the nozzle are grid independent.

Similarly, it was necessary to choose a value for δt in the correlated models that was solution independent. As in the previous chapter, it is recommended that the value of δt be some fraction of the eddy lifetime. In the case of a round jet, there is a wide range of scales throughout the solution domain, and it was determined that setting $\delta t < 20\%$ of the eddy lifetime yielded an independent solution for the dispersion predictions. For the remainder of the calculations, δt was set to 10% of the eddy lifetime, updated every time a new velocity fluctuation is sampled to adjust to the changing dynamics of the flow.

The fluid simulations were calculated using the $k - \epsilon$ turbulence model, since the implementation of the second order closure model offered in CFX-TASCflow proved to be problematic in the case of a round jet. The computational mesh used in the rest of the calculations consisted of 80 nodes in the axial direction with an expansion factor of 2%, and 81 nodes on both of the cross-stream axes with an expansion factor of 2.8%. Expansion factors were used to concentrate nodes in the potential core of the jet.

For the particle tracking measurements, the flow solution was interpolated onto a mesh that consisted of 19360 nodes. This procedure was required to satisfy the memory constraints implicit in calculating the Reynolds stresses using an eddy viscosity assumption in the CFX-TASCflow particle routine code for input in the anisotropic particle dispersion models.

6.3 Results

An important property of a turbulent round jet is that the radial velocity profiles become self-similar at a certain downstream position. This is usually taken as 30 jet

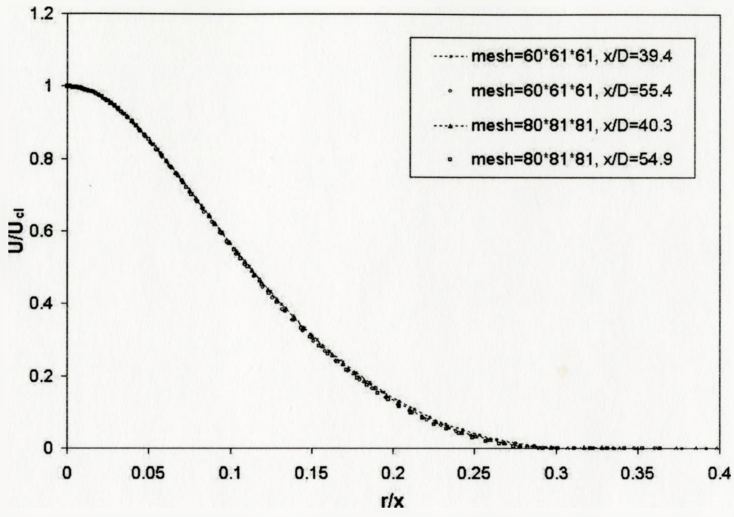

FIGURE 6.2: Radial velocity profiles for two different meshes

diameters downstream of the nozzle (Hussein *et al.*, 1994). Goertler estimated the velocity profile in the fully developed region by the following expression (White,1991):

$$\frac{U}{U_{cl}} = \left[1 + 57.76\left(\frac{r}{x}\right)^2\right]^{-2} \tag{6.1}$$

In Figure 6.3 the predictions of the CFX-TASCflow code are plotted along with Goertler's expression and data from Yuu *et al.* A characteristic width called the half-radius, $r_{0.5}$, is used to indicate the spread of the jet. The half-radius is the value of the r at which the fluid velocity is half the centerline value, that is $U/U_{cl} = 0.5$, and it varies linearly with downstream distance. The predicted half-radius from Goertler's solution is 0.0847. The numerical prediction gives a half-radius of 0.111, thus overestimating the half-radius by approximately 31.1%.

The jet's nozzle in the simulation was square and the experiment was for a round jet. Since the numerical solutions indicate a similar solution to the round jet solution, the assumption taken seems to be valid. However, it is difficult to ascertain whether the selection of hydraulic diameter contributed to the error in half-width prediction.

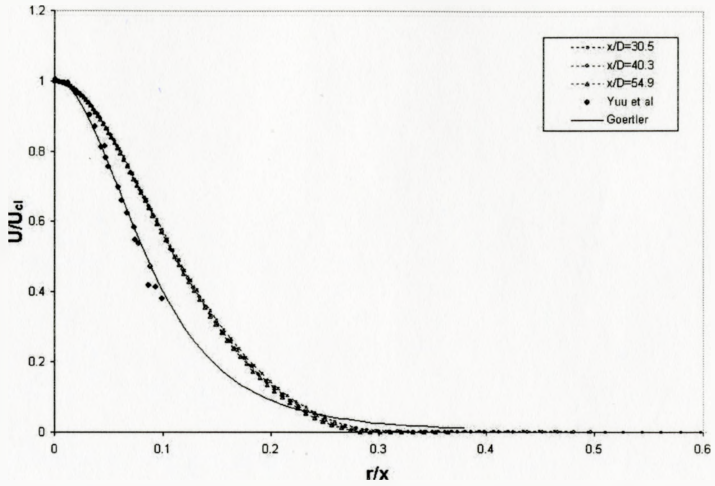

FIGURE 6.3: Similarity Solution

It is shown in Figure 6.4 that the numerical prediction overpredicts the axial velocity decay of the round jet. This is consistent with the the overprediction of the half-radius of the jet. As a result, it will be impossible to obtain clear conclusions about the performance of the particle dispersion models since they will be subjected to a spurious fluid flow field.

Since the CFX-TASCflow code injects particles independently into the computational domain, it is important to ensure that enough particles are injected to yield an independent dispersion profile. Three particle quantities of 32000, 64000 and 128000 were injected using the model of Hennick & Lightstone (see Figure 6.5). It is clear that all three quantities give similar particle concentration profiles, and it was concluded that 64000 particles would be sufficient to generate the particle data for the simulation of this experiment.

The results of the model of Shuen, Chen and Faeth for the various downstream locations are plotted in Figure 6.6. The results are similar for all downstream locations, and are in good agreement with the results published by Yuu *et al.* However, since

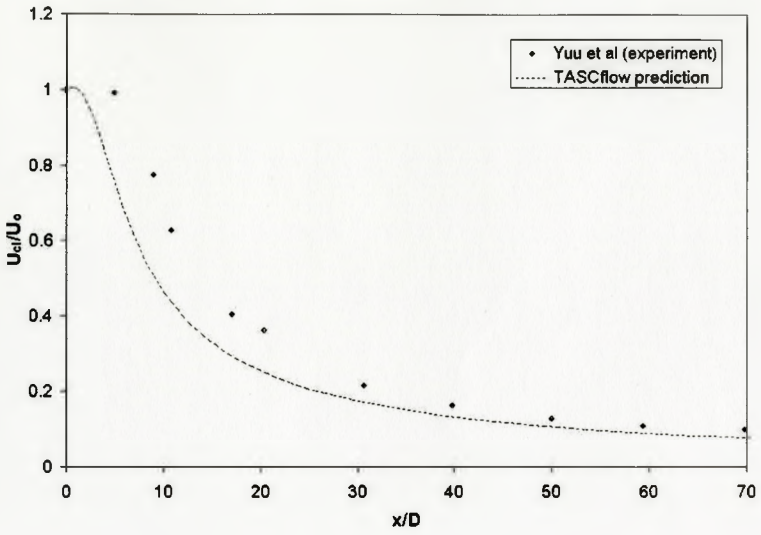

FIGURE 6.4: Axial velocity distribution of the aerodynamic field

the fluid solution prediction for half-width was over-predicted, the spread of the jet was exaggerated in the simulation and the fluid velocities in the outer radial regions of the jet were higher then in the experiment, consistent with the over-prediction of the jet centerline decay. It is therefore reasonable to assume that the particle dispersion predictions would be greater if the correct flow field had been used. This is because the majority of particles in the outer radial regions were convected rapidly downstream by the higher axial velocities that they were exposed to, and did not have the time to disperse as much as they might have. As a result, it is thought that the model of Shuen, Chen and Faeth would over-predict the dispersion of particles if subjected to the correct velocity field.

The results of the model of Hennick & Lightstone are shown in Figure 6.7. The results are once again similar for the four downstream locations. In this case, the concentration of particles is under-predicted in the region near the centerline, but the dispersion is over-predicted for values of $r/z > 0.12$.

The results for the model of Zhou & Leschziner are shown in Figure 6.8. The results

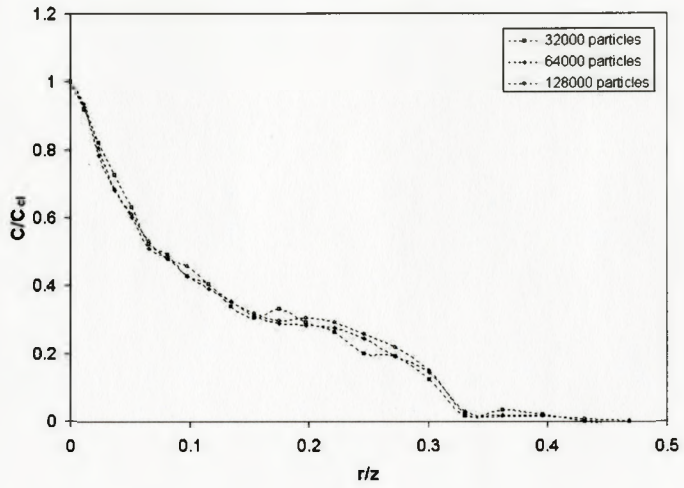

FIGURE 6.5: Particle number independence test

are also similar for the four downstream locations, as per the theory. The profile is in good agreement in the near-centerline region, but tends to over-predict the dispersion in the region of $r/z > 0.15$. As before with the model of Shuen *et al.*, it is surmised that the profiles would be over-predicted if the flow field solution used had correctly matched the data of Yuu et al.

The results for the proposed model of Evinou and Lightstone are presented in Figure 6.9. The results are under-predicted in the region $r/z < 0.1$. It is forwarded that the results in this region are under-predicted in relation to those of the Zhou & Leschziner model since the incorporation of the spatial auto-correlation function has damped the radial dispersion of the particles, which are expected to lag the dispersion of a fluid point as per the crossing-trajectory theory. Although, it is impossible to conclude authoritatively, it is possible that the proposed model would have done a good job capturing the experimental behaviour of the particles with the correct velocity field and the inclusion of the spatial correlation.

Finally, the axial decrease of particle concentration can be seen for all models in

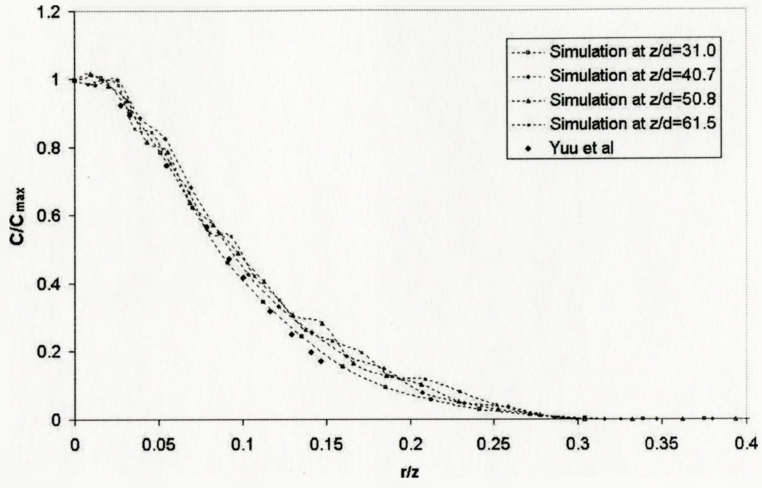

FIGURE 6.6: Concentration profiles using the model of Shuen, Chen and Faeth

Figure 6.10. The models of Hennick & Lightstone and Shuen *et al.* both do a good job of capturing the centerline decay of particle concentration. The model of Zhou & Leschziner slightly under-predicts the centerline concentration, indicative of an exaggerated dispersion. Contrasted, the proposed model of Evinou and Lightstone over-predicts the centerline concentration. This is most likely due to the inclusion of the spatial correlation function to model the crossing trajectory effect of the particles. It is possible that if the tests were re-run with the correct flow field solution, the results for the proposed model would yield a better fit to the experimental data.

6.4 Conclusions

This study compared the numerical results obtained from five different particle dispersion models with experimental data for a dust-laden, turbulent round jet presented by Yuu *et al.*. The CFD code CFX-TASCflow was unable to correctly capture the flow field solution as given experimentally by Yuu *et al.* and an expression by Goertler.

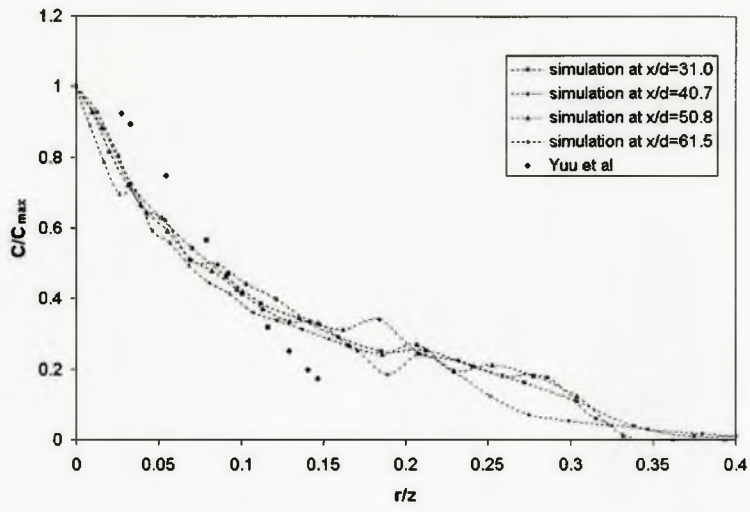

FIGURE 6.7: Concentration profiles using the model of Hennick and Lightstone

The four particle models of Shuen, Chen and Faeth, Hennick and Lightstone, Zhou and Leschziner and the proposed model of Evinou and Lightstone were run for the case of $U_o = 20m/s$ and $d_p = 15\mu m$. It was shown that the model of Shuen, Chen and Faeth gave the best results for the downstream concentration profiles. It was conjectured that since the half-radius of the round jet was over-predicted by the numerical solution, the particle data was under-predicted as a result of the particles being convected downstream too quickly. Therefore, it is plausible that the model of Evinou and Lightstone would have generated results close to the experimental data had the correct flow field solution been captured.

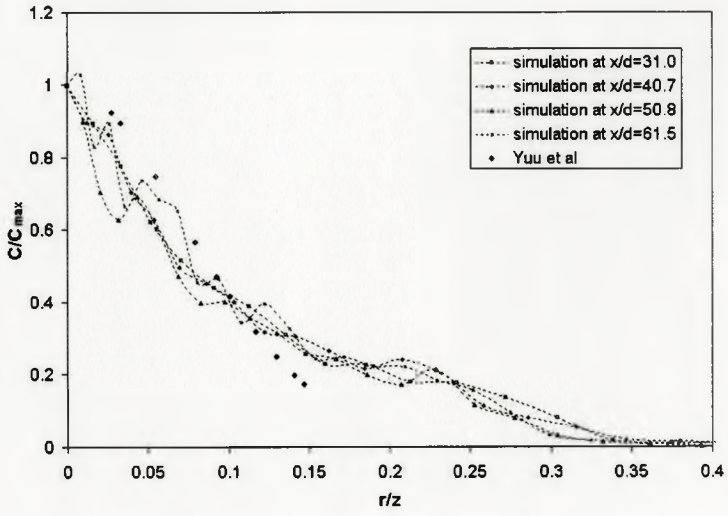

FIGURE 6.8: Concentration profiles using the model of Zhou and Leschziner

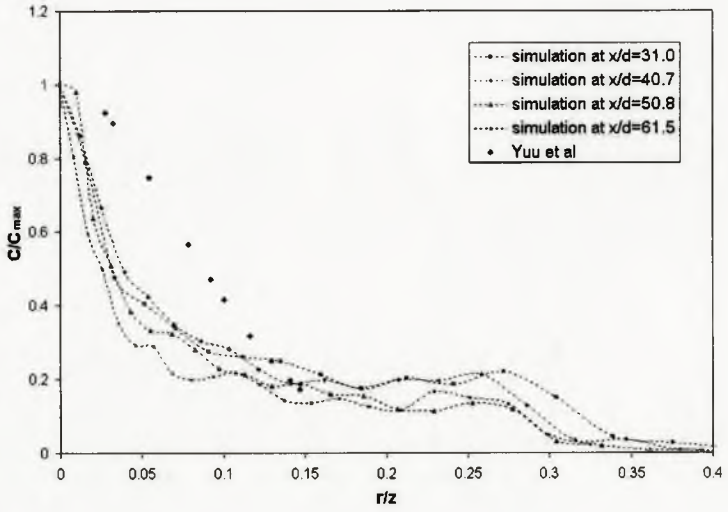

FIGURE 6.9: Concentration profiles using the model of Evinou and Lightstone

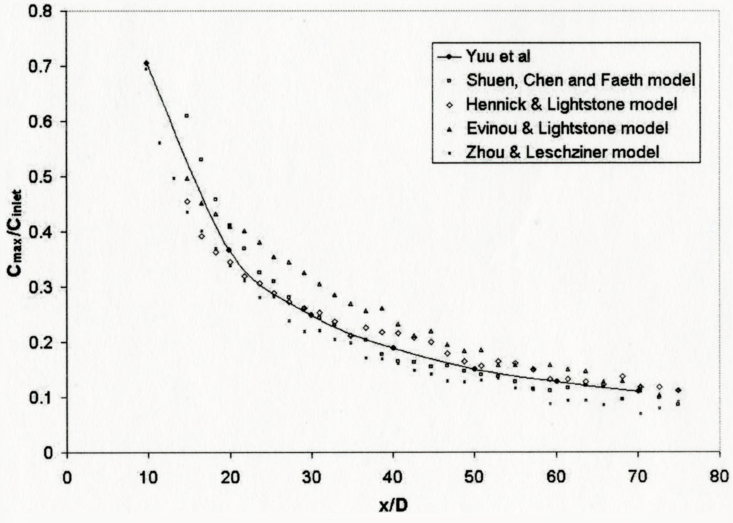

FIGURE 6.10: Maximum cross-stream concentration for all models

CHAPTER 7

The Experiment of Hishida, Maeda et al, 1993

The mathematical models of Shuen, Chen and Faeth, Hennick & Lightstone, the anisotropic model of Zhou & Leschziner and the proposed model of Evinou and Lightstone are applied and compared with experimental data for the case of a multiphase, incompressible, turbulent shear layer. The experimental conditions used in these simulations are the same as those reported in Hishida *et al.* (1992). The experiment was simulated using the CFX-TASCflow CFD code. Measurements of particle velocity and dispersion were compared to results generated by each model considered in this thesis.

The chapter begins with a description of the experiment. The numerical simulation is described, and the predictions of each model are presented. Results are discussed in detail.

7.1 Description of Experiment

The experiment of Hishida *et al.* was performed in a two-dimensional, vertical turbulent shear layer wind tunnel. The experimental flow configuration can be seen in Figure 7.1. The flow was diverted into two streams and passed through a settling

nozzle and merged at the point of the trailed edge of the splitter plate. The splitter plate was made of two thin aluminum plates, which were 0.3 mm thin, and had a constant spacing of 0.57 mm.

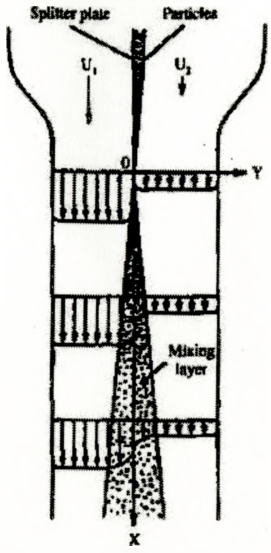

FIGURE 7.1: Experimental flow configuration (Hishida *et al.*,1992)

Measurements of the particle number density and mean velocity profiles at four positions (100, 150, 200 and 250mm) downstream from the edge of the plate were taken. The flow is vertical and downward, thus gravity acts to accelerate the particles. In the paper of Hishida *et al.*, the experimenters considered three flow conditions. These are presented in Table 7.1. These different conditions were employed to clarify the effects of the particle residence time, particularly with reference to the bulk velocity, which is given by $U_b = (U_1 + U_2)/2$. In condition (I), the bulk velocity is 17m/s, and in condition (II), it is 8.5m/s. Only conditions (I) and (II) will be examined in this work.

The properties for the three kinds of glass particles used in this experiment can be found in Table 7.2. The particles were injected at the initial point of the mixing layer and were given exit velocities much different then those of the flow to generate large

TABLE 7.1: Flow conditions

Condition	U_1 [m/s]	U_2 [m/s]
(I)	21	13
(II)	13	4
(III)	15	3

relative velocities. The exit velocities for the particles were approximately $1.1m/s$ for $U_b = 17m/s$ and $0.9m/s$ for $U_b = 8.5m/s$. The experimenters were particularly interested in determining the effects of particle residence time on particle dispersion, which is a function of the relative velocity between the gas and the particulate. Hishida *et al.* investigated whether the air phase was modified by the presence of the particles, and found that the maximum difference between the two velocity profiles in a single-phase and in two phases was very small. They therefore concluded that turbulence modulation due to the presence of the particles was insignificant for the particle mass flow rates used in this experiment (Hishida *et al.*,1992).

TABLE 7.2: Particle Properties

Mean Diameter d_p (μm)	Mass Flow Rate $\dot{m}(g/s)$	Density $\rho(kg/m^3)$	Relaxation Time (sec)
42	7.5	2590	0.014
72	20.9	2590	0.041
135	20.4	2590	0.144

7.2 Description of Boundary Conditions and Simulation

Since the flow in this experiment is two-dimensional, it was possible to model the control system in a manner that made efficient use of control nodes. The duct was made to be $3.5m$ long and $1m$ high. Nodes were placed on the x and y axes with expansion factors to concentrate nodes in the regions of maximum gradient (i.e. along the centerline and in the developing region). Only three nodes were used in the z direction, since the flow was symmetric in this direction. Symmetry boundary conditions were applied on the top, bottom and side walls of the duct (see Figure 7.2). Sensitivity studies examining different heights for the duct showed that the symmetry boundary conditions at the top and bottom of the duct did not influence the solution of the flow field for heights greater then 0.75 m.

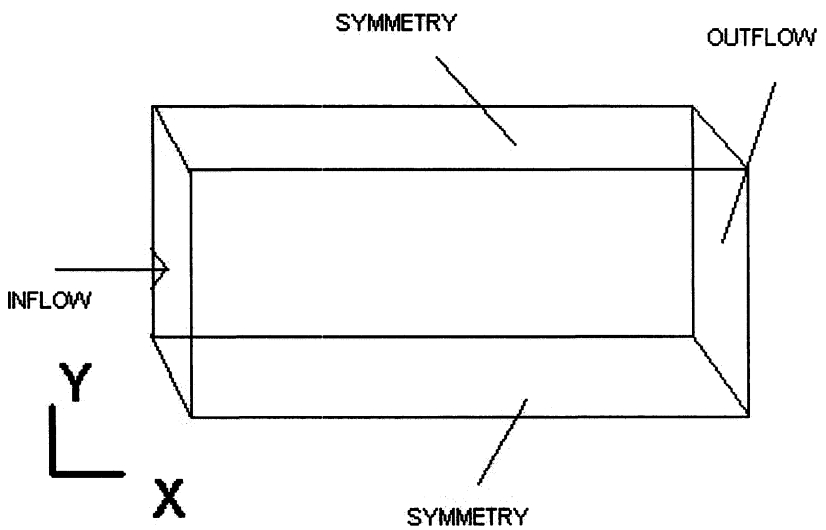

FIGURE 7.2: Description of Boundary Conditions

An important consideration when undertaking a numerical investigation of this nature, is to ensure that the solution the CFD code generates is independent of grid

size. As such, a coarse grid and fine grid solution was modeled for this solution where the number of nodes used in each direction was effectively doubled. The coarse grid solution consisted of 120 nodes in the axial direction, 3 nodes in the symmetric direction, and 101 nodes in the transverse direction. The fine mesh solution consisted of 240,3, and 201 nodes, respectively. Figure 7.3 demonstrates that both meshes generate similar profiles for the axial velocity of the flow. Figure 7.4 shows similarity for tranverse velocity. Figures 7.5 and 7.6 show similarity for the two turbulent quantities of interest, the turbulent kinetic energy and the turbulent dissipation. The remainder of the calculations in this section were completed using the coarse grid for efficiency purposes.

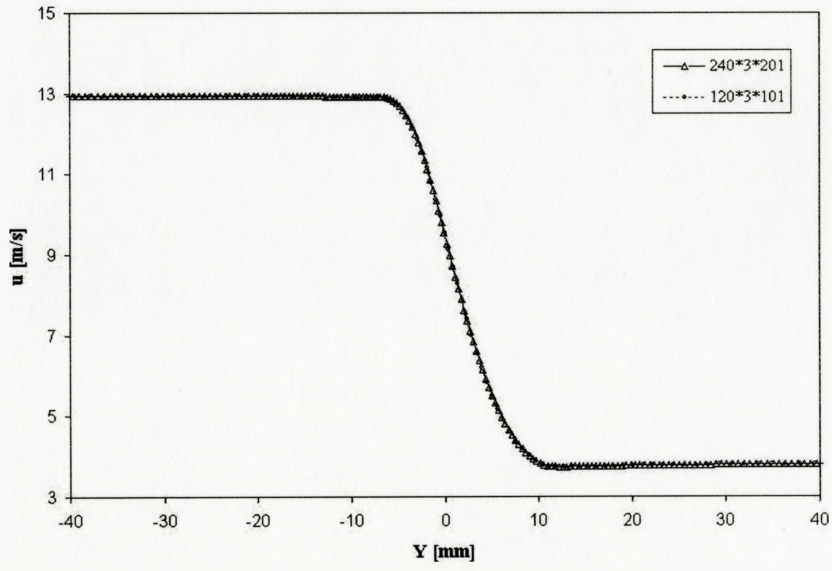

FIGURE 7.3: Grid Independence of Axial Velocity at $X = 100mm$

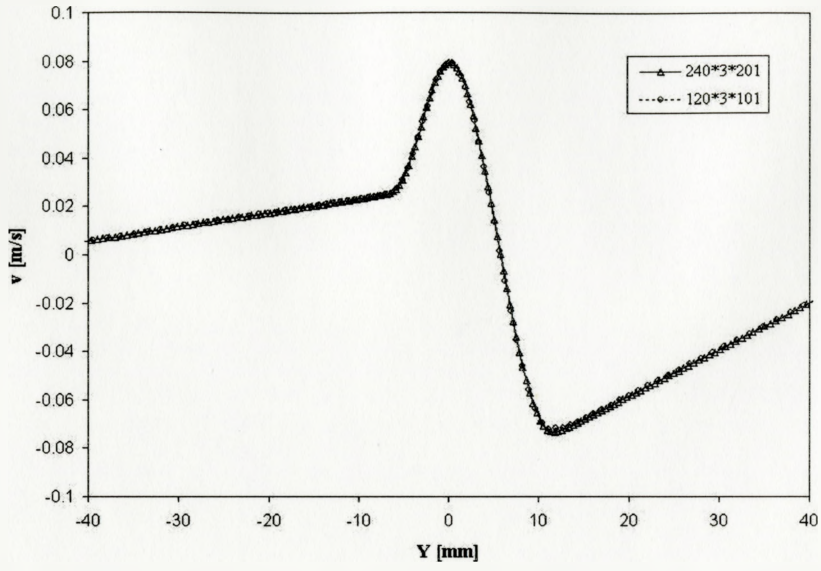

FIGURE 7.4: Grid Independence of Transverse Velocity at $X = 100mm$

7.3 Results

Before the experiments for particle trajectories were undertaken, it was imperative that the flow field solution obtained using the second moment closure model was verified. To verify the flow field solution, the distributions of mean velocity were plotted at several downstream locations. The splitter plate produces a small velocity defect, but at positions in the region past x=50mm, the distributions of the mean velocities approach a hyperbolic tangent curve (see Figure 7.7). The mean velocity profiles are normalized along the x-axis by two variables. The first is $Y_{0.5}$, which is defined as the cross-stream location where the magnitude of the fluid velocity is equal to the small velocity U_2 plus half of δU. The second variable is the integral momentum thickness, which is given by

$$\delta_{iu} = \int_{-\infty}^{\infty} \frac{\overline{u_g} - \overline{u_2}}{\overline{u_1} - \overline{u_2}} \left(1 - \frac{\overline{u_g} - \overline{u_2}}{\overline{u_1} - \overline{u_2}}\right) dy \tag{7.1}$$

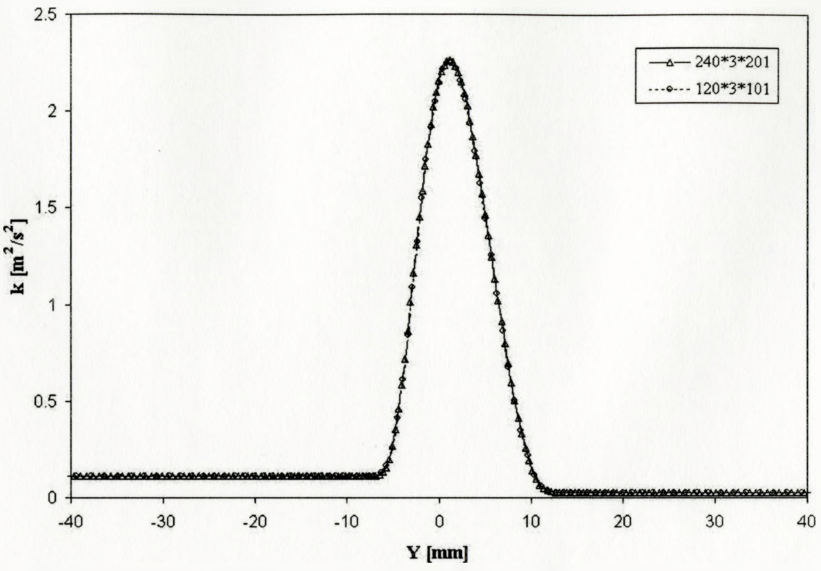

FIGURE 7.5: Grid Independence of Turbulent Kinetic Energy at $X = 100mm$

It is particularly interesting to look at the predictions for half-width growth by the second-order closure models as compared to the experimental data for $U_b = 8.5m/s$ and $U_b = 17m/s$, as seen in Figure 7.8. The half width is defined by Hishida *et al.* as the lateral distance from the point of $U_f = 0.75\Delta U + U_2$ to that of $U_f = 0.25\Delta U + U_2$. It can be seen that in both cases, the second order closure scheme tends to under-predict the half-width at all down-stream locations. This is important, since it should have a profound effect on the particle dispersion data that will be examined later in the chapter.

The average error for half-width prediction by the second order closure model is 32% under-prediction for $U_b = 8.5m/s$, and 23% under-prediction for the case of $U_b = 17m/s$. The second order closure model was used in the calculations because accurate predictions for the Reynolds stresses were required for the anisotropic particle dispersion models. Coimbra *et al.* showed that the $k - \epsilon$ model generates better predictions for the growth of the shear layer; however, it was impossible to generate

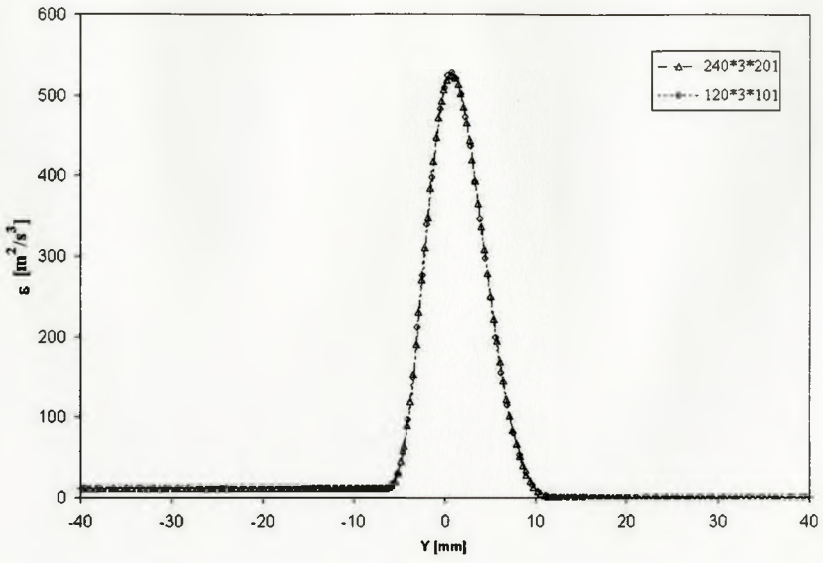

FIGURE 7.6: Grid Independence of Turbulent Dissipation Rate at $X = 100mm$

the Reynolds stresses using the eddy viscosity assumption and the $k - \epsilon$ model in TASCflow for this case due to memory constraints.

7.4 Particle Dispersion Validation

Before the individual models can be assessed, it is necessary to determine the appropriate time step (i.e. δt) necessary for the correlated models, as well as the number of particles that must be injected per simulation to generate statistically meaningful dispersion profiles.

As was described earlier, the correlated models of Hennick and Lightstone, Zhou and Leschziner, and the proposed correlated model of Evinou and Lightstone, generate velocity flow fluctuations that are correlated in time. As such, the time step, δt, over which velocity fluctuations are held correlated is of great importance. The general

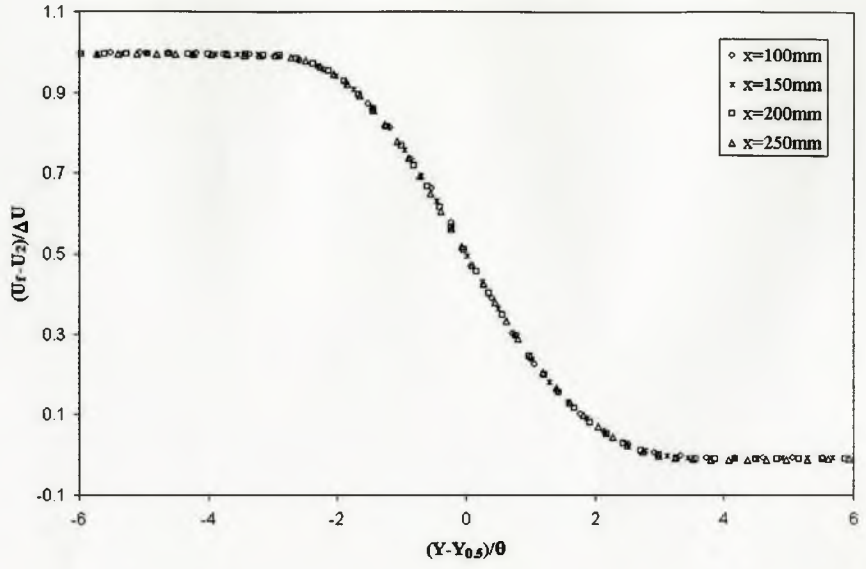

FIGURE 7.7: Distribution of mean velocities in single-phase flow for condition (I)

idea is that δt should be some fraction of the eddy integral time scale, given by $\tau_{LI} = 0.135 \cdot k/\epsilon$. For the case of $U_b = 8.5m/s$, the average integral time scale in the computational domain was calculated to be approximately $0.002s$. Hennick & Lightstone showed that a relative fraction of 5% to 10% of the integral time scale tends to be sufficient to achieve "time step independence". Therefore, it is projected that an appropriate δt for this investigation should be of the order 0.0001s.

The model of Hennick & Lightstone was run for a range of δt ranging from 0.00005s to 0.01s to validate that the code was generating particle dispersion profiles that were time step independent of the order predicted by the theory. The test case of $U_b = 8.5m/s$ and $d_p = 42\mu m$ was examined for this purpose, and 4000 particles were injected to create the particle dispersion profiles at the downstream location $X = 250mm$. This location was chosen far downstream of the inlet to ensure that the predictions for the different time steps were independent of the inlet concentration, which was the same in all the cases. It is clear from Figure 7.9 that the particle

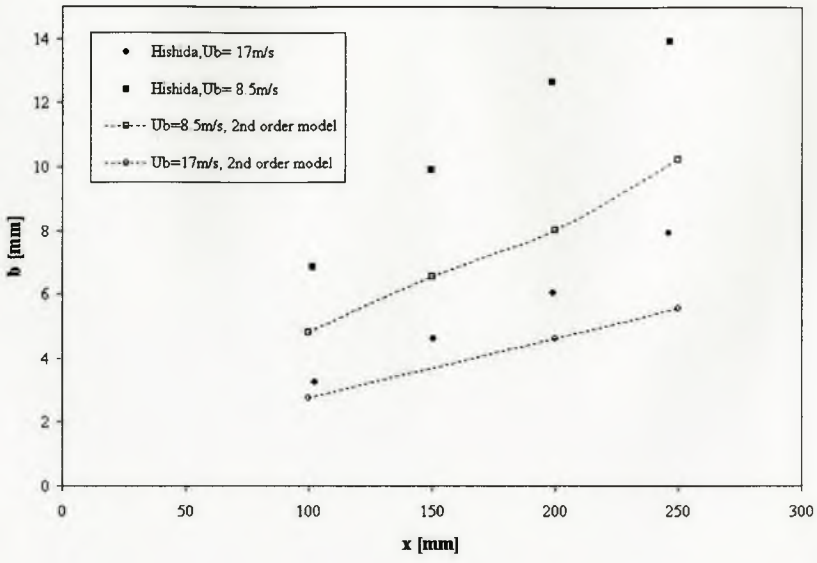

FIGURE 7.8: Numerical Predictions of Half-widths

concentrations approach independence for a time step of 0.0002s and less. This is in accordance with the theory.

It was also necessary to validate the coding of the model equations for the different correlated models. This process will be outlined for the model of Hennick & Lightstone As was mentioned earlier, the model of Hennick & Lightstone samples correlated velocities according to the relation:

$$u_i' = R(\delta t)R(\delta x)u_{t-\delta t}' + e_t \tag{7.2}$$

The nature of the correlation in this relation essentially states that as δt approaches zero, the new velocity fluctuation will be highly correlated to the velocity fluctuation seen in the previous computational time step, and inversely, as δt grows large, the correlation of the velocity fluctuations at subsequent time steps will disappear, and the new velocity fluctuation will be a random variable. Figure 7.10 shows the relationship

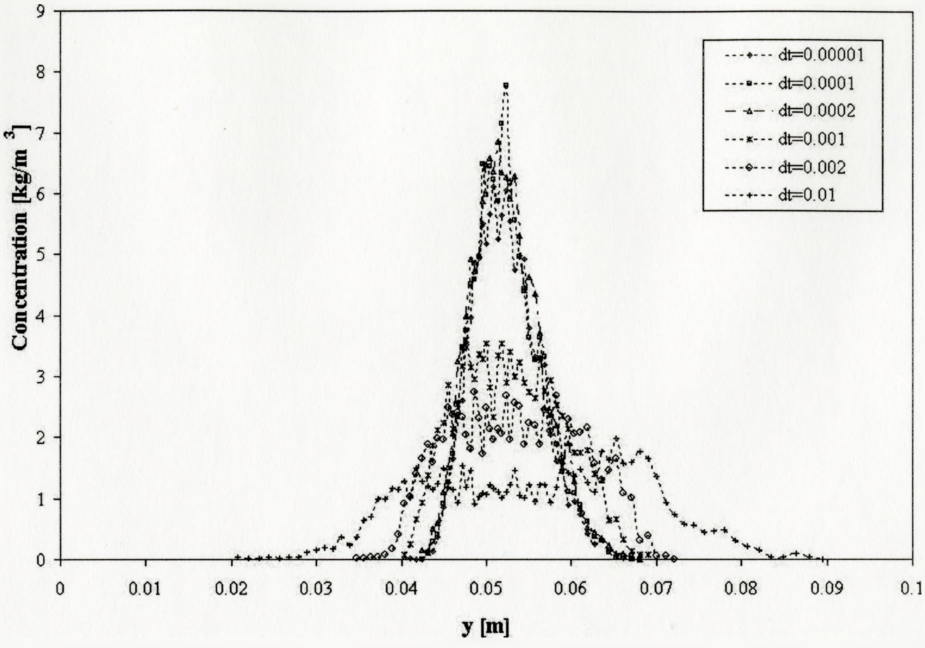

FIGURE 7.9: Validation of Appropriate Time Step

between the magnitude of the random component of the fluctuating velocity as a function of the correlation function, $R(\delta t)$. As explained earlier, this figure clearly shows that the magnitude of the random contribution, e_t, decreases as $R(\delta t)$ increases, or more precisely, as the value of δt grows smaller. More specifically, as δt gets small, the fluctuating velocities at successive time steps become highly correlated, and the effects due to randomness during the time step disappear, which is in accordance with the theory.

The final procedure that needs to be verified before the models can be properly assessed is determining the number of particles required to produce significant dispersion data. CFX-TASCflow generates particle concentrations by injecting and tracking particles one at a time. The particles do not interact with each other, and in the case of the Hishida experiment, do not affect the fluid solution. A minimum number of

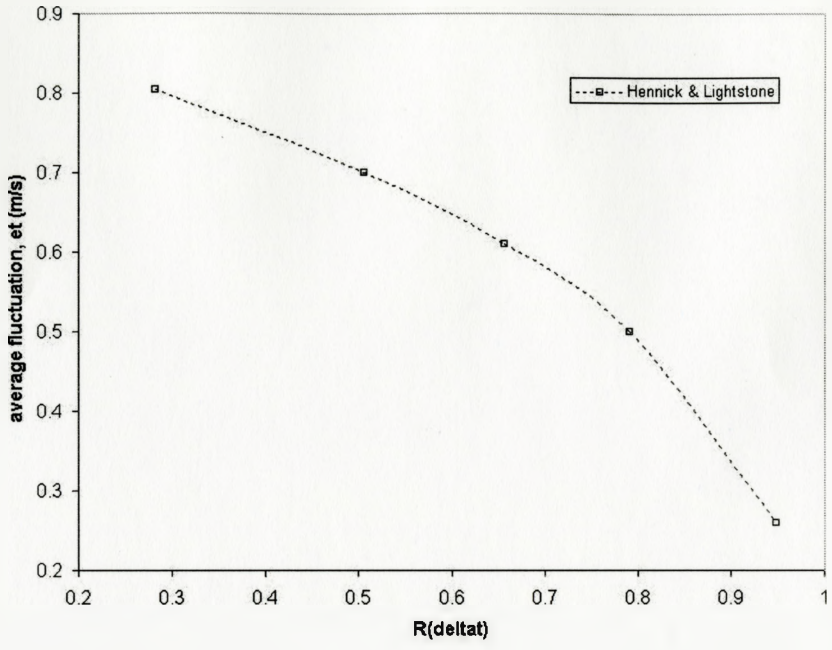

FIGURE 7.10: Magnitude of e_t as a function of $R(\delta t)$

particles must be injected for any given flow to give a statistically significant dispersion profile. For the case of $U_b = 8.5m/s$ and $d_p = 42\mu m$, 24000, 32000 and 40000 particles were injected, and dispersion profiles were acquired at a downstream location of $X = 200mm$ using the particle model of Hennick & Lightstone. From the data in Figure 7.11, it is clear that these three amounts give graphically similar particle dispersion profiles, and the solutions are therefore independent of particle number. As a result of this study, it was concluded that 32000 particles would be sufficient to generate meaningful data for the cases studied in the subsequent sections.

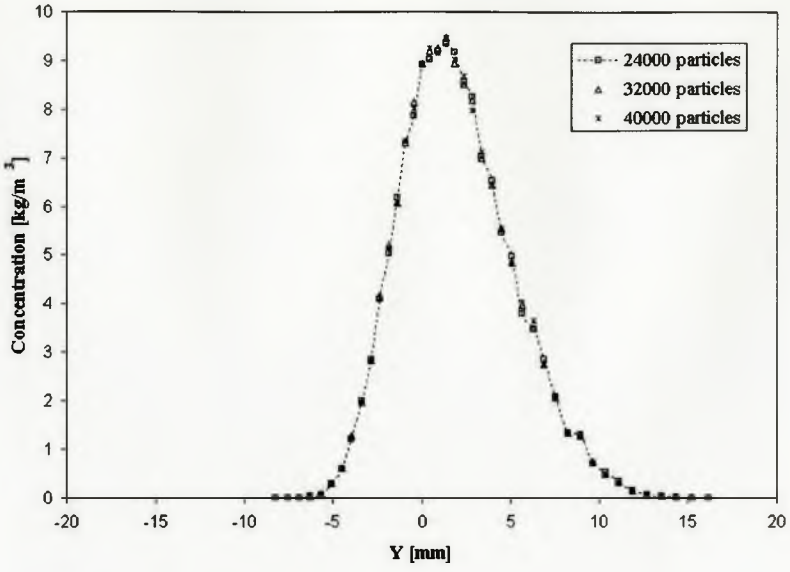

FIGURE 7.11: Particle concentration profiles for three different particle injection quantities at $X = 200mm$

7.5 Particle Dispersion Data

The first case that was examined was for $U_b = 8.5m/s$ and $d_p = 42\mu m$. All four models were run with 32000 particles and, for the correlated models, a time step of $\delta t = 0.0001$. The distributions over the cross-section at $X = 250mm$ are presented in Figure 7.12. In the experiment, it can be seen that the particle velocities are close to that of the single-phase at this downstream location. All four models have under-predicted this phenomenon.

The distributions over the cross-section at $X = 100mm$ and $X = 250mm$ are presented in Figures 7.13 and 7.14. From Figure 7.13, it is clear that all four of the models have under-predicted the spread of the particles at the downstream location of $X = 100mm$. This can partly be attributed to the error in prediction of the half-width of the flow field solution. There is a definite progression with respect to the spread prediction of the models. The SCF model predicts the least amount of particle

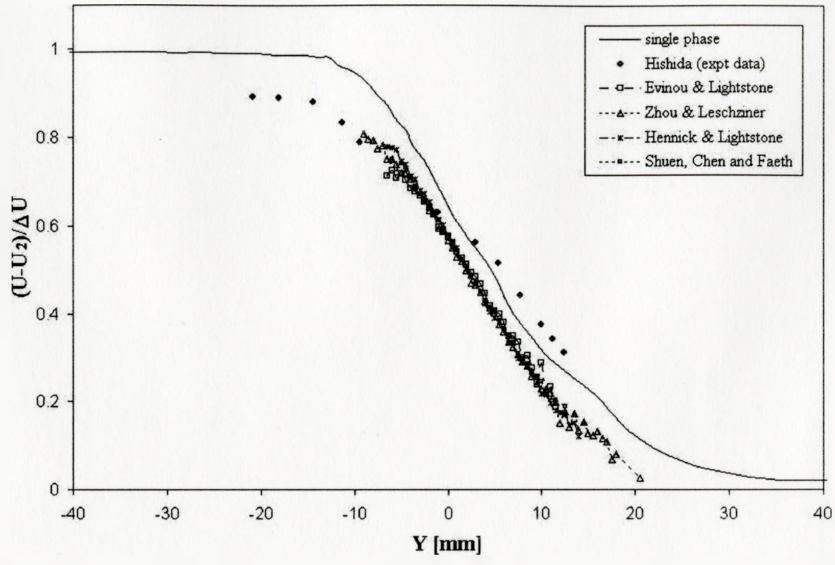

FIGURE 7.12: Cross-sectional distributions of particle mean velocities at $X = 250mm$ for $U_b = 8.5m/s$ and $d_p = 42\mu m$

dispersion. The proposed model of Evinou and Lightstone has a slightly larger spread, but is significantly less then the model of ZL. The model of Hennick & Lightstone falls between the two anisotropic models.

Further downstream at $X = 250mm$, similar patterns between the models can be seen in Figure 7.14. It should be noted that the concentrations in this plot have been normalized by the peak concentration value from the downstream location of $X = 100mm$. Since the experimenters did not provide data for this parameter, the calculated data was normalized by the peak concentration from each of the model's prediction at $X = 100mm$. Again, the model of Zhou & Leschziner tends to have the closest comparison to the experimental data, and then, in order of decreasing accuracy, the models of Hennick and Lightstone, Evinou and Lightstone, and finally, Shuen, Chen and Faeth.

In order to determine magnitudes of error in the different model's predictions for

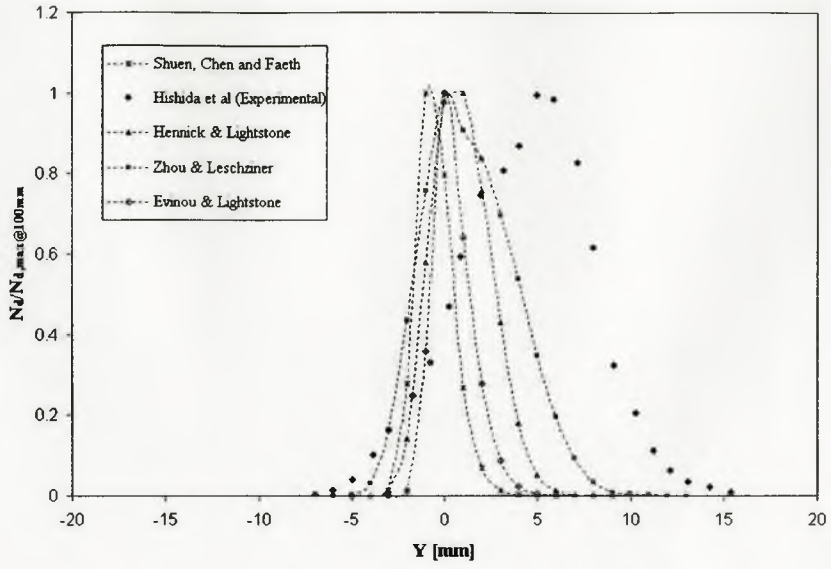

FIGURE 7.13: Particle Number Density Distributions at $X = 100mm$ for $U_b = 8.5m/s$ and $d_p = 42\mu m$

particle dispersion, it is useful to look at a plot of the variance of the displacement, $\overline{y^2}$ at different downstream locations. To evaluate the particle dispersion from the particle number density profile, $\overline{y^2}$ is calculated using the following equation:

$$\overline{y^2} = \frac{\int N_d \cdot y^2 dy}{\int N_d dy} \tag{7.3}$$

where N_d is the local particle number density. The variations of particle mean square displacements for the four different models as compared to the data collected by Hishida *et al.* can be seen in Figure 7.15. It is abundantly clear from this plot that all four models have had a significant difficulty in accurately predicting the particle dispersion. The model of Zhou & Leschziner comes closest to the experimental data, but still has an error of 84.4%. The model of Hennick & Lightstone is next closest, with an associated error of 91.2%, followed by the proposed model of Evinou and Lightstone with an error of 96% and Shuen, Chen and Faeth with an error of 97%.

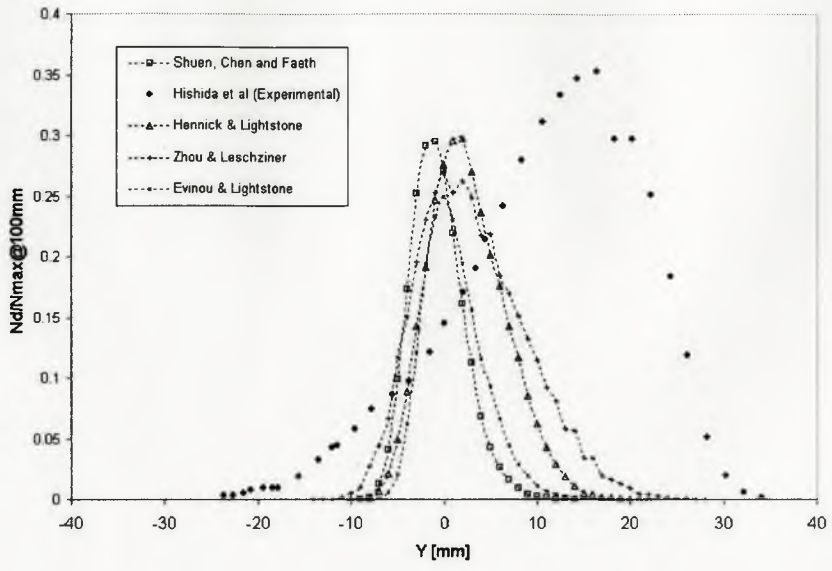

FIGURE 7.14: Particle Number Density Distributions at $X = 250mm$ for $U_b = 8.5m/s$ and $d_p = 42\mu m$

It should be remembered that the fluid solution under-predicted the growth of the half-widths of the flow by approximately 30%, so the under-prediction of the models is not as significant as these errors indicate.

In Figure 7.16, the stream wise particle velocity fluctuations at the downstream location can be seen. It can be seen that the experimental particles have basically 'caught up' to the fluids, and exhibit essentially the same mean fluctuations at the fluid at this downstream location. Of the particle models examined, it is clear that the Zhou & Leschziner outperforms the other models. The Shuen *et al.* model is the least capable of capturing the axial fluctuations of the particle. This is due to the fact that this model is isotropic in nature, and is 'unaware' that the turbulent fluctuations are larger in this direction. Again, it can be seen that the new model of Evinou and Lightstone significantly 'lags' behind the model of Zhou & Leschziner which it is mostly based on.

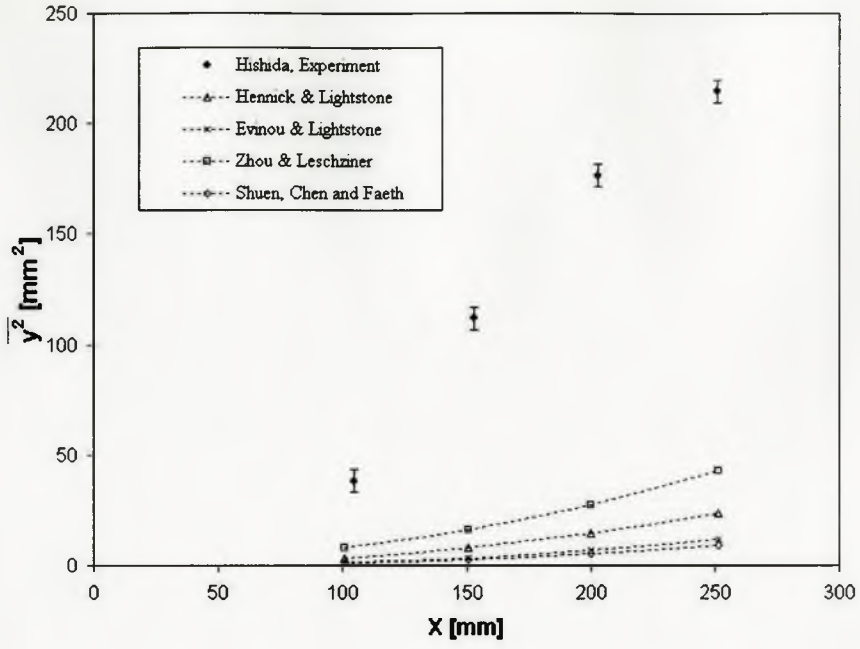

FIGURE 7.15: Variations of particle mean square displacement for $U_b = 8.5m/s$ and $d_p = 42\mu m$

Figure 7.17 examines the cross-stream velocity fluctuations of the particles. These fluctuations must be captured correctly if the dispersion is to be predicted accurately. Experimentally, it can be seen that the particles of Hishida *et al.* do not quite reach the peak of the fluid phase fluctuations at this downstream location. Of the four models examined, the model of Zhou & Leschziner once again comes closest to matching the experimental predictions. It is interesting to note that the predictions of the new model of Evinou and Lightstone are the furthest from the experimental values, since it outperformed the model of Shuen *et al.* in the prediction of the $\overline{y^2}$ terms.

These results are consistent with the findings of Coimbra *et al.*, who found that the particle velocity fluctuations (both longitudinal and cross-stream) are underpredicted for this experiment all across the shear layer using stochastic separated flow

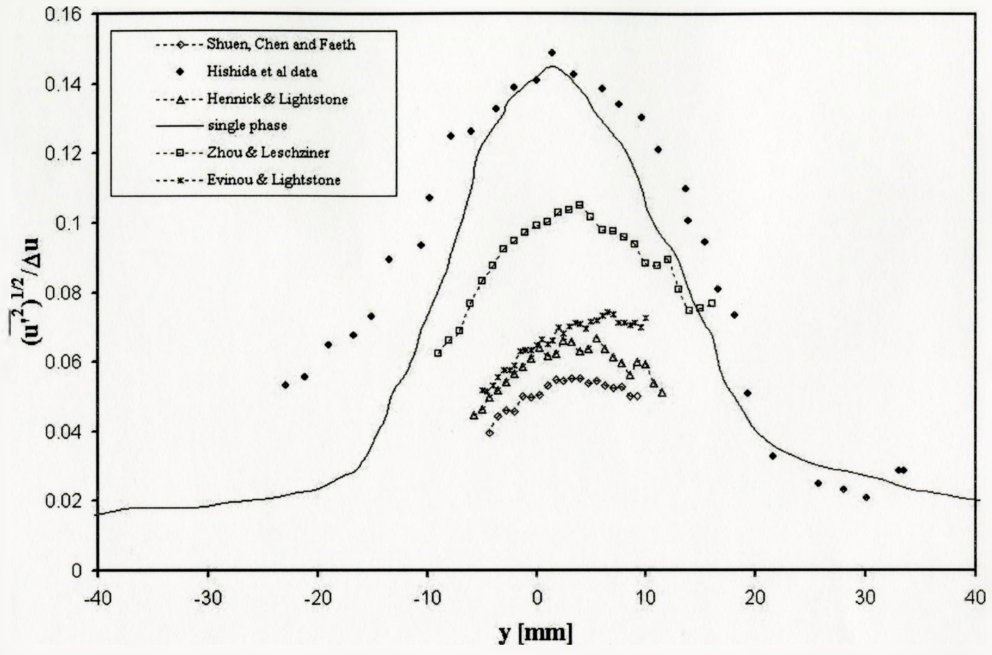

FIGURE 7.16: Particle streamwise velocity fluctuation at $X = 250mm$ for $U_b = 8.5m/s$ and $d_p = 42\mu m$

algorithms. They used an isotropic particle dispersion model similar to the model of Shuen *et al.*, and an algebraic model used to simulate the anisotropy of the flow. Coimbra *et al.* attributed the high particle velocity fluctuations observed experimentally to particle interactions with large unsteady, vortical structures in the shear layer.

The second case that was examined was the case for $U_b = 8.5m/s$ and $d_p = 135\mu m$. The particles in this case are roughly 3 times as large as those in the first case. As a result, the particles will be less likely to respond quickly to the changes in the fluctuating velocity of the fluid, due to the increased particle relaxation time. Essentially, these particles require more energy to respond to the changes in fluid velocity due to their increased mass, and as a result, take a longer time to accelerate or de-accelerate to the new fluid velocity. As well, the crossing trajectory effect (CTE)

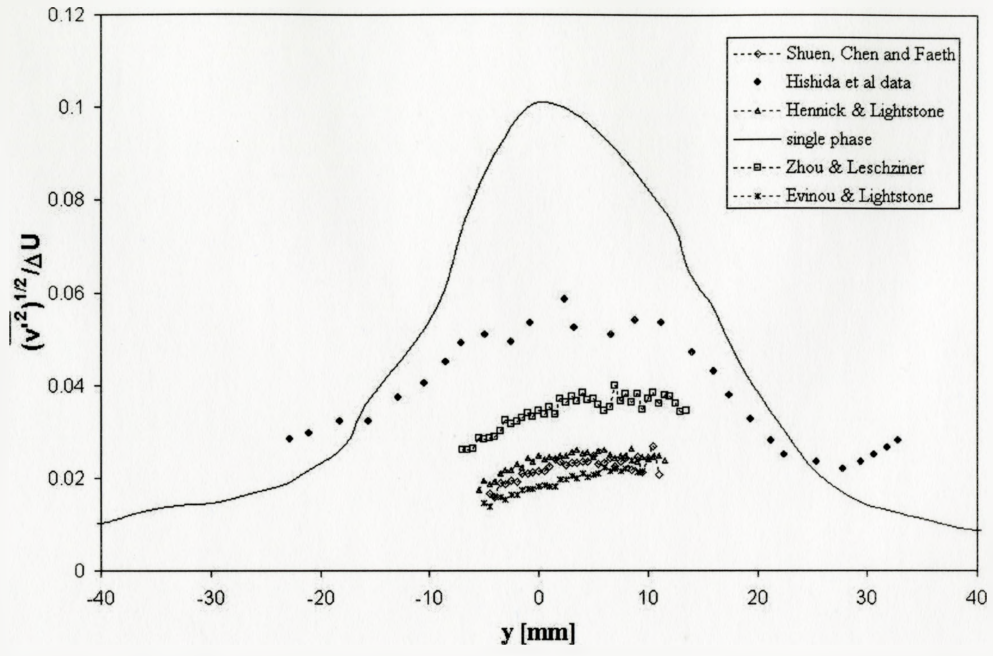

FIGURE 7.17: Particle cross-stream velocity fluctuation at $X = 250mm$ for $U_b = 8.5m/s$ and $d_p = 42\mu m$

will be much more important in this case, and it is thought that the proposed model of Evinou and Lightstone will perform well since this effect is taken into account in the derivation of the new model.

As before, the first variable that will be examined is the mean particle velocity prediction. All four models predict particle velocities that are well within the experimental data (see Figure 7.18). It is clear from this figure that all four models are still under-predicting the spread of particles quite drastically, however,the magnitude of the velocities predicted is admirable.

In Figure 7.19, the predicted value for $\overline{y^2}$ is plotted. From this data, it is possible to discern the magnitude of the error in dispersion prediction. The model of Zhou & Leschziner generates a prediction that is closest to the experimental data set, but

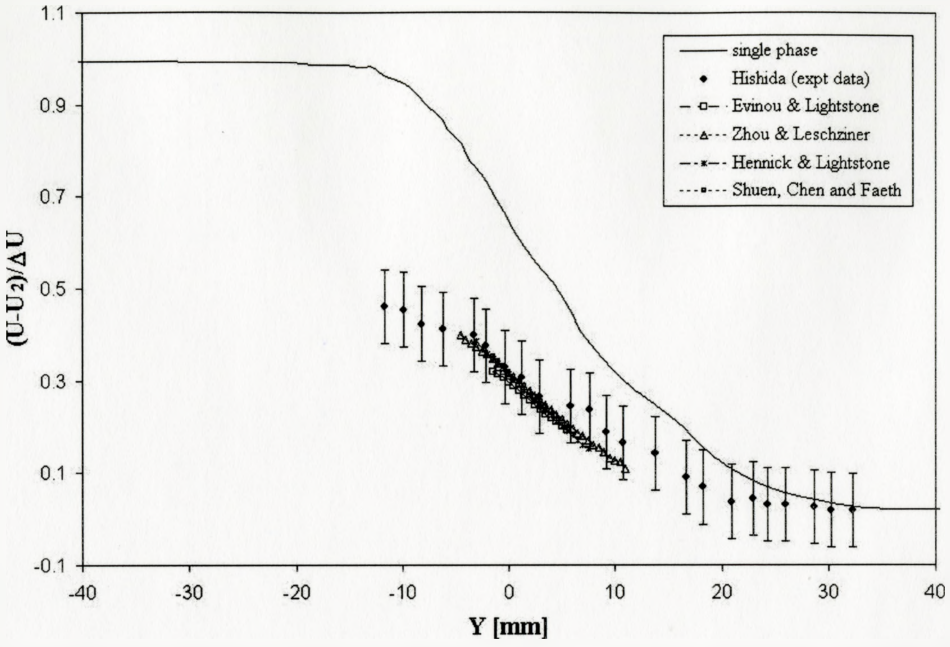

FIGURE 7.18: Cross-sectional distributions of particle mean velocities at $X = 250mm$ for $U_b = 8.5m/s$ and $d_p = 135\mu m$

is 61.2% in error. As before, the model of Hennick & Lightstone tends to generate better predictions then the two final models, but still has an error of 88.4%. It was thought that the proposed model of Evinou and Lightstone would do a better job with the larger particles because of the consideration of the CTE; however, it appears that the elimination of the Frenkiel functions in the correlation functions has had an overwhelming negative effect, when compared to the model of Zhou & Leschziner. The EL model has an error of 93.7% for this case. The model of Shuen, Chen and Faeth performs only slightly better, with an average error of 92.3% for $\overline{y^2}$.

Despite the error, it can clearly be seen that the dispersion of the larger particles is significantly smaller then the dispersion of the small particles from the previous case (as seen in Figure 7.15). Physically, the larger particles do not respond to the turbulent fluctuations as quickly as the smaller particles due to much larger particle

relaxation times; and because of this the trajectories of the larger particles follow the streamlines of the flow closely. It was conjectured that the modeling of the crossing-trajectory effect would have a more profound effect on the results, but it can be seen that the incorporation of the CTE in the proposed model of Evinou and Lightstone has not had the desired effect.

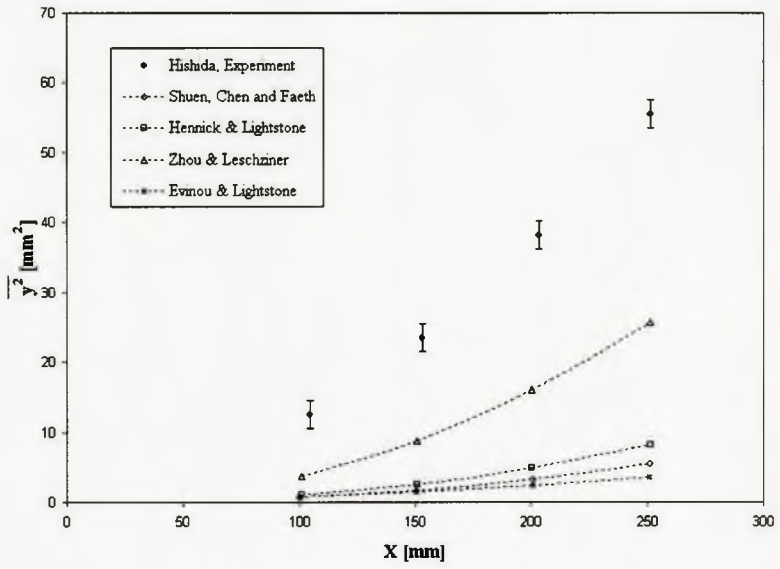

FIGURE 7.19: Variations of particle mean square displacement for $U_b = 8.5m/s$ and $d_p = 135\mu m$

From the predictions for particle stream wise velocity fluctuations, as shown in Figure 7.20, it can be seen that the model of Zhou & Leschziner very nearly falls within the error range of the experimental data for $\overline{u^2}$. Of the three remaining models, the proposed model of Evinou and Lightstone generates the best predictions. This is most likely due to the fact that this model has taken the anisotropy of the flow into account. The discrete eddy model of Shuen *et al.* continues to perform poorly.

Finally, the model of Zhou & Leschziner generates the best predictions for the particle fluctuating velocity in the cross-stream direction, $\overline{v^2}$, as seen in Figure 7.21. These

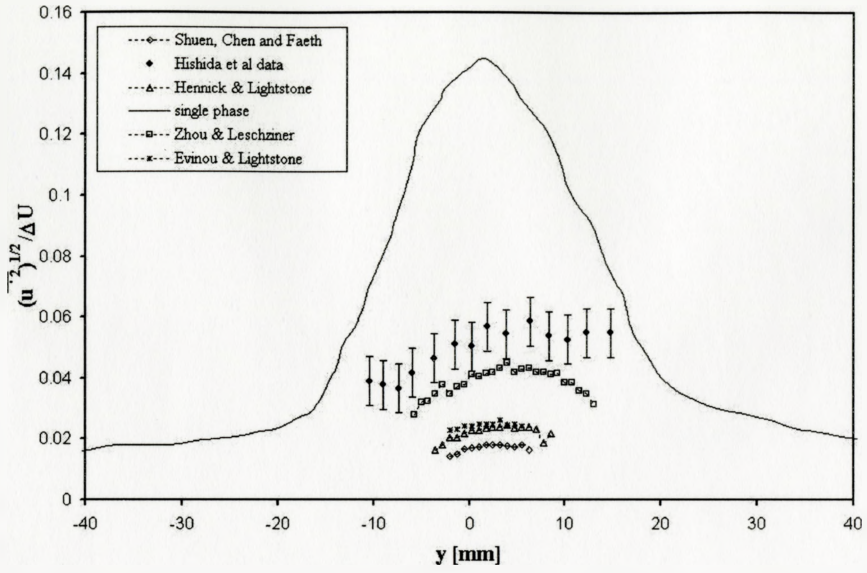

FIGURE 7.20: Particle streamwise velocity fluctuation at $X = 250mm$ for $U_b = 8.5m/s$ and $d_p = 135\mu m$

results come very close to falling within the error range of the experimental data of Hishida *et al.*. There is not much difference between the predictions of the other three models.

The final case that will be examined is for particle sizes of $d_p = 42\mu m$ again, but for a bulk velocity of $17m/s$. As the Reynolds number of this flow will be greater then in the first two cases, the turbulence intensity of the flow will be greater, and thus the variation in predictions for instantaneous gas velocity between the models should be greater. As a result, this case should be very revealing in terms of strengths and weaknesses of the models under study. An additional circumstance of the higher bulk velocity is that the particles will be convected through the computational domain by the mean flow at a greater rate in this case, and therefore the dispersion is expected to be much less then in the previous cases.

As before, the first parameter to be examined is the particle mean velocity at $X =$

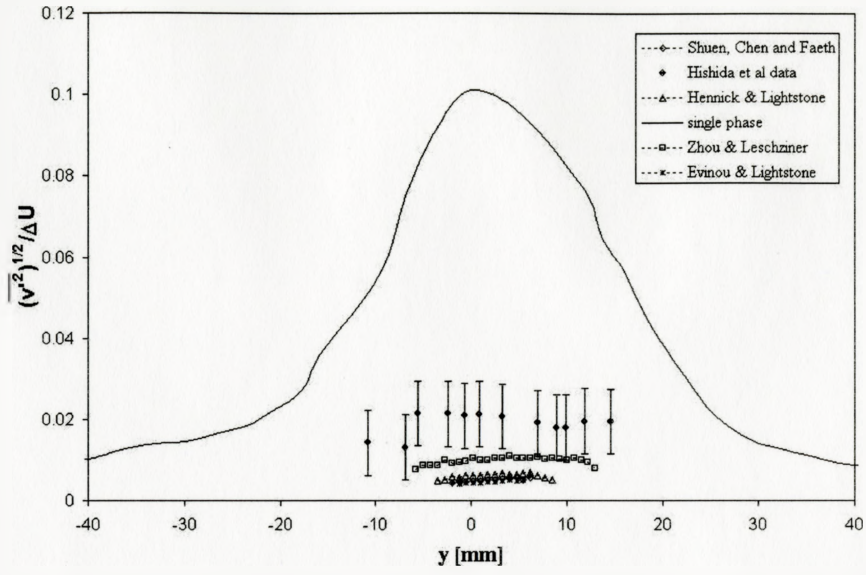

FIGURE 7.21: Particle cross-stream velocity fluctuation at $X = 250mm$ for $U_b = 8.5m/s$ and $d_p = 135\mu m$

$250mm$ downstream of the injection point, as seen in Figure 7.22. It can be seen immediately that all four models have had difficulty capturing the width of dispersion that is evident in the experimental results. However, the magnitudes of the particle mean velocities seem to be in accordance with the experimental data.

As in the first case, it is possible to examine the particle number density profiles. As shown in Figure 7.23, the model of Zhou & Leschziner has actually over-predicted the dispersion profile of the experiment at the initial downstream location of $X = 100mm$. Similar to previous results, the model of Hennick & Lightstone produces the next best results, followed by the proposed model of Evinou and Lightstone, and finally by the model of Shuen *et al.*

At the downstream location of $X = 250mm$, the model of Zhou & Leschziner has been overtaken by the experimental result, but generates a prediction that quite close to the data (see Figure 7.24). The model of Hennick and Lightstone generates a

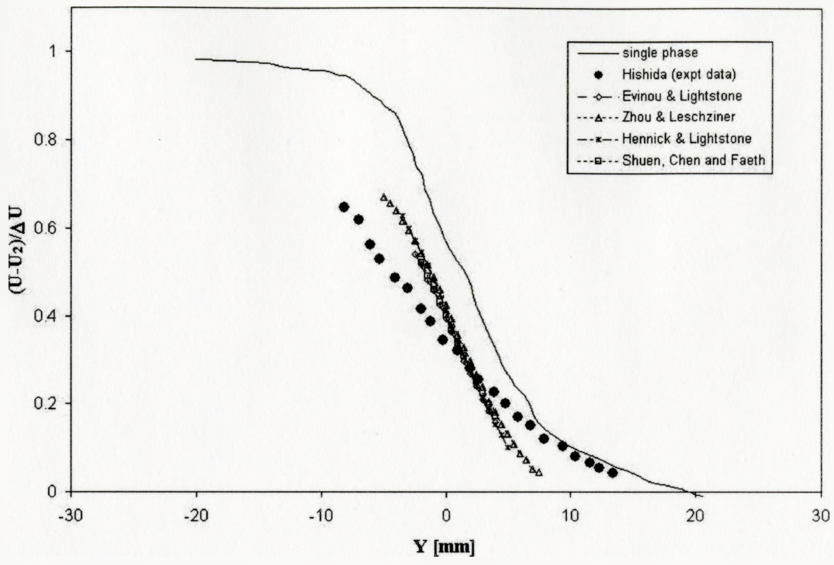

FIGURE 7.22: Cross-sectional distributions of particle mean velocities at $X = 250mm$ for $U_b = 17m/s$ and $d_p = 42\mu m$

reasonable profile, while the other models produce predictions that are severely under predicted.

For the higher bulk velocity in this case, it can be seen that the magnitudes of $\overline{y^2}$ with X are much smaller then those for $U_b = 8.5m/s$. Hishida *et al.* explain that these differences are due to the difference in particle residence time. A larger relative velocity causes a shorter particle residence time and less effect of the vortical structural motion, causing a decrease in dispersion (Hishida *et al.*,1992). In terms of the modeling of the flows, this can be described as the particles being quickly convected through the domain before they get a chance to be dispersed. The model of Zhou & Leschziner once again comes closest to the experimental data set, with an under prediction of 30%. The model of Hennick and Lightstone has an error of 58%, followed by the model of Evinou and Lightstone at 71% and the discrete eddy model of Shuen, Chen and Faeth with an error of 80%.

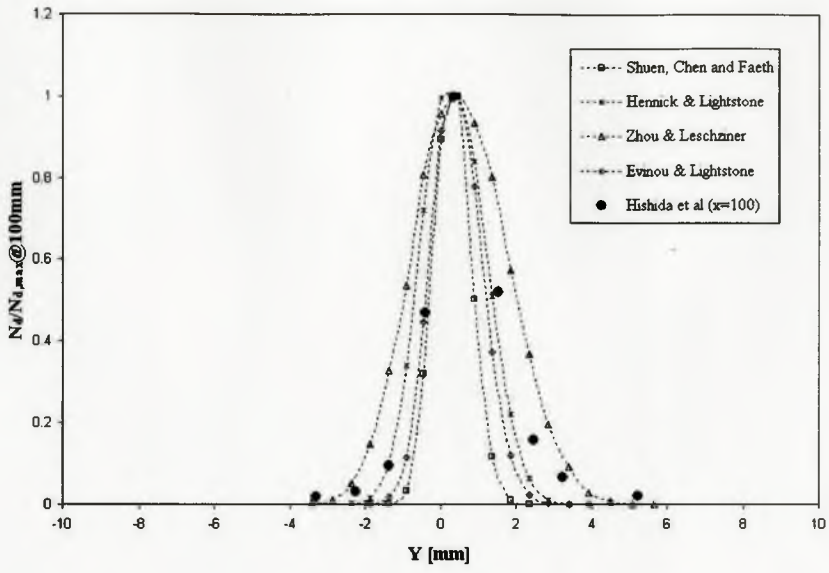

FIGURE 7.23: Particle Number Density Distributions at $X = 100mm$ for $U_b = 17m/s$ and $d_p = 42\mu m$

It is also of interest to examine the model predictions for the two fluctuating velocities, $\overline{u_p^2}$ and $\overline{v_p^2}$. Figure 7.26 shows the stream wise particle fluctuations at the downstream location of $X = 250mm$. It can be seen that the predictions of the model of Zhou & Leschziner very nearly falls within the error range of the experimental data for $\overline{u^2}$. Of the three remaining models, the proposed model of Evinou and Lightstone generates the best predictions. The model of Shuen *et al.* continues to perform poorly.

Finally, the model of Zhou & Leschziner generates the best predictions for the particle fluctuating velocity in the cross-stream direction, $\overline{v^2}$, as seen in Figure 7.27. These results come very close to falling within the error range of the experimental data of Hishida *et al.*. There is not much difference between the predictions of the three other models.

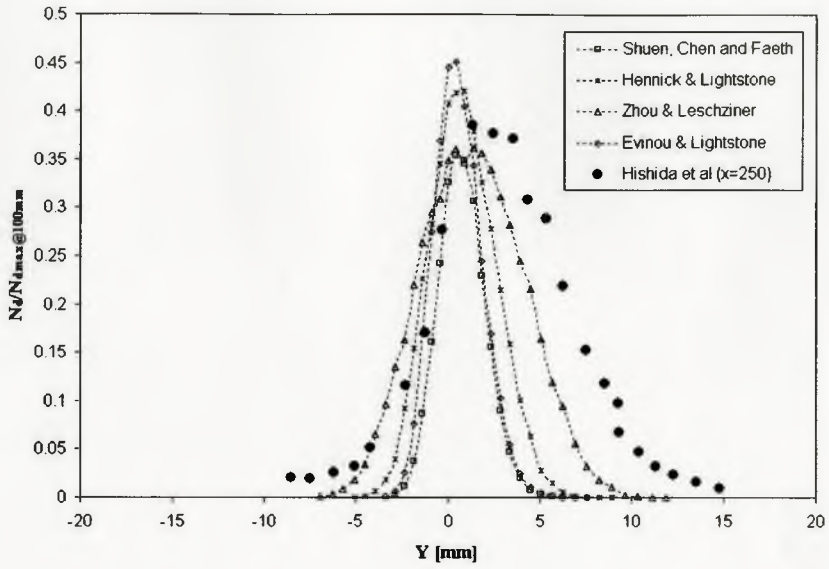

FIGURE 7.24: Particle Number Density Distributions at $X = 250mm$ for $U_b = 17m/s$ and $d_p = 42\mu m$

7.6 Conclusions

This study compared the numerical results obtained from four different particle dispersion models with experimental data for a turbulent mixing layer. The four stochastic separated flow models considered were the discrete eddy model of Shuen, Chen and Faeth, the time-correlated model of Hennick & Lightstone, the anisotropic, correlated model of Zhou & Leschziner, and the proposed model of Evinou and Lightstone, an anisotropic, correlated model that accounts for the crossing trajectory effect. The models were tested for two different bulk velocities of the mixing layer, and also for two different particle sizes, to study the effects of particle residence time and the influence of particle relative velocities on model performance.

The models were able to adequately predict the magnitude of mean particle velocities at different downstream positions. Particle dispersion or spread, in contrast, was significantly under-predicted. This could be due in part to the inability of the fluid

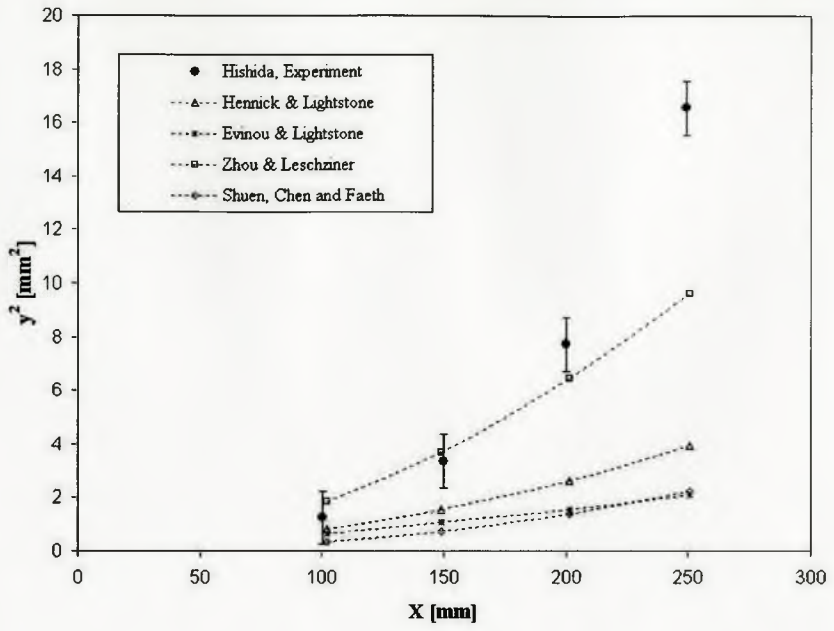

FIGURE 7.25: Variations of particle mean square displacement for $U_b = 17m/s$ and $d_p = 42\mu m$

flow solver to accurately predict the half-width of the flow field. The anisotropic model of Zhou & Leschziner was best able to predict the dispersion of particles, as evidenced by the magnitude of error for the calculated prediction of $\overline{y^2}$ for the different cases. The model of Shuen *et al.* was the least capable of predicting this value, perhaps because of the model's discrete eddy assumption, that the particle's are subjected to one fluid fluctuating velocity for the length of its interaction with an eddy. This is in contrast to the other models assumption that the particle will be subjected to a series of correlated fluctuating velocities during the interaction with the eddy.

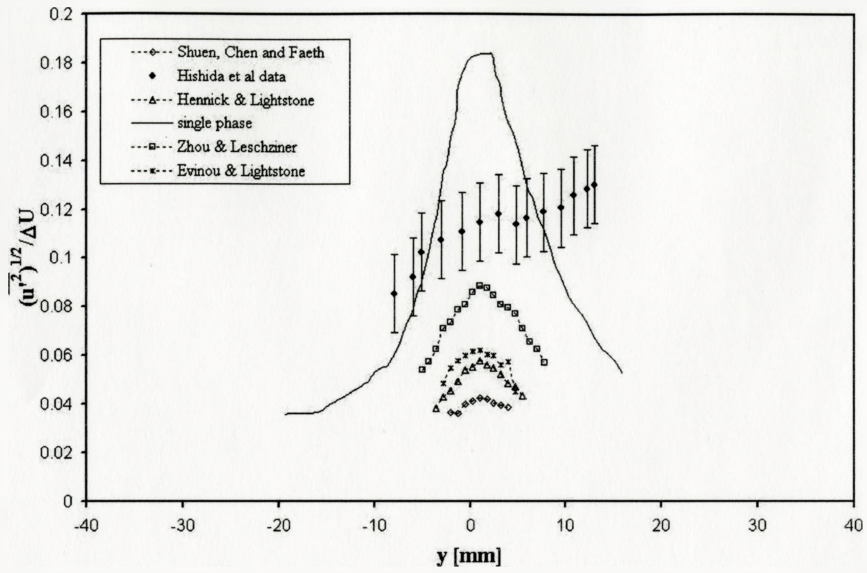

FIGURE 7.26: Particle stream wise velocity fluctuation at $X = 250mm$ for $U_b = 17m/s$ and $d_p = 42\mu m$

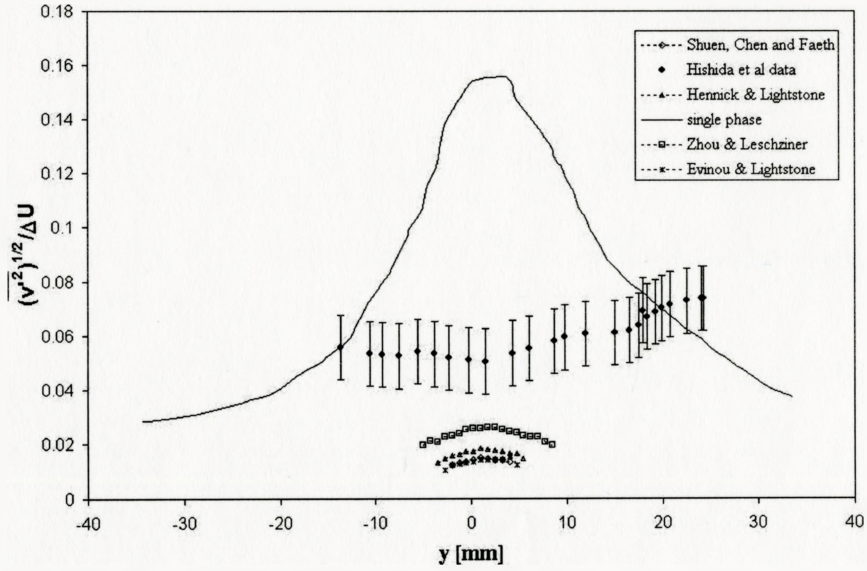

FIGURE 7.27: Particle cross-stream velocity fluctuation at $X = 250mm$ for $U_b = 17m/s$ and $d_p = 42\mu m$

CHAPTER 8

Closure

8.1 Summary and Conclusions

This research has focused on the problem of particle dispersion in turbulent shear flows. The particle dispersion problem is intrinsically linked to turbulence, most specifically, the modelling of instantaneous turbulent gas fluctuations. It is helpful to think of particles being convected by the mean flow of the fluid, and dispersed from the streamlines of the fluid phase by the instantaneous turbulent fluctuations.

A popular process to solve the problem has been the use of discrete eddy models. Discrete eddy models assume that a particle will be 'captured' by an eddy for a finite length of time during which it will be exposed to the instantaneous velocity of the eddy. The trajectory of the particle will then be determined by solving a Lagrangian equation of motion for the particle which takes into account drag and gravitational forces. Research on this topic by Shuen *et al.* and Gosman & Ioannides has proven very promising, and their models have been incorporated into many commercial CFD packages, such as CFX-TASCflow.

While the discrete eddy models offer good computational affordability, the assumption that a particle will be exposed to only one fluctuating velocity during its interaction time with an eddy is erroneous. Researchers such as Zhou & Leschziner have proposed correlated models where a particle is subjected to a series of correlated fluctuating

velocities as it traverses an eddy. The model of Zhou & Leschziner uses a temporal correlation based on an approximation suggested by Hinze:

$$R(\delta t) = \exp\left(\frac{-\delta t}{T}\right)$$

Hennick & Lightstone furthered this model by introducing a spatial correlation to take into account the crossing trajectory effect; which concerns particles that have large relaxation times and don't respond quickly to changes in the fluid velocity. This correlation acts to correct for the fact that a particle and a fluid point will not end up in the same spot after a period of time, which is an inherent assumption of the Zhou & Leschziner temporal model.

All of the previous models were isotropic models; that is they assumed that the turbulence acted in equal intensity in all directions. For the case of turbulent shear flows such as mixing layers and jets, the turbulence tends to be very directional or anisotropic. Zhou & Leschziner (1991b) were one of the first researchers to present an anisotropic, time-correlated model. The fluctuating gas velocities are a function of the fluctuating velocities in each direction at a previous time step, and take into account the directional correlation in space reflected by the anisotropy of the Reynolds stresses.

Berlemont *et al.* and Burry & Bergeles suggest anisotropic correlated models that account for the crossing-trajectory effect by including a spatial Eulerian correlation with a Frenkiel form. Lightstone shows that the use of Frenkiel correlations results in an effective asymptotic correlation that is exponential in shape and clearly different from the intended correlation, and therefore does not recommend their usage. As a result, this work was focused on introducing an anisotropic model that uses a temporal, spatial correlation that accounts for the crossing-trajectory effect without utilizing Frenkiel functions.

In order to assess this proposed model, several particle dispersion experiments were selected from the literature. The first experiment was the shear layer experiment of Lazaro & Lasheras. This case looked at a jet stream mixture of air with water droplets exiting in a room filled with quiescient air. This experiment was used by Zhou & Leschziner in the validation of their time-correlated anisotropic model, and their data was used as a benchmark for the process. The second case was a round jet experiment conducted by Yuu *et al.*. The final case was a shear layer experiment by Hishida *et al.* with two streams of air at different velocity that interact at the end of a splitter plate where the particles are injected.

The performance of the proposed model was assessed by comparison with the experimental data and with the predictions of three of the previously mentioned models. The models chosen for comparison were the Shuen, Chen and Faeth discrete eddy model, the Hennick and Lightstone isotropic temporal and spatially correlated model and the Zhou and Leschziner anisotropic temporally correlated model. These models were chosen as a broad representation of the field of research.

The CFD code CFX-TASCflow was found to have difficulties accurately predicting the flow field solution for the shear layer experiments. The code, using the second moment closure model of Launder, Reece and Rodi, consistently underpredicted the growth rate of the shear layer. This error induced further error in the particle dispersions data found from the models. As a result, it was difficult to properly assess the performance of the models.

In the experiment of Lazaro & Lasheras (1989), all four models predicted similar particle concentration growth rates. The growth rates were severely underpredicted compared to the experimental data, which can partly be explained due to the underprediction of the growth of the fluid shear layer. Another reason for the error is due to the inability of the second moment closure algorithm to model the effects of particle interactions with the large, unsteady vortical structures that exist in shear

layers, as suggested by Coimbra *et al.*.

In the experiment of Yuu *et al.* (1978), the $k - \epsilon$ closure model was used to obtain the flow field solution. The half-radius, $r_{0.5}$, was over-predicted by about 30%, which most likely resulted in the dispersion profiles being underpredicted for the four models examined. While the discrete eddy model of Shuen, Chen and Faeth came closest to matching the experimental data, it was surmised that the proposed model of Evinou and Lightstone would have performed well if the correct fluid flow behaviour had been captured.

The shear layer experiment of Hishida *et al.* (1992) was also simulated using the four models outlined earlier. This experiment differed from that of Lazaro & Lasheras in that the particles originated from a small nozzle in the center of two fluid streams at a much different velocity from the fluids, in order to induce large relative velocities. As a result, the particle models generated significantly different predictions for the different particle cases in the experiment. The anisotropic model of Zhou & Leschziner generated the predictions that were closest to the experimental data. The proposed model of Evinou and Lightstone did not perform as well as the model of Zhou & Leschziner, most likely due to the fact that the Eulerian spatial correlation that was incorporated into the model consistently acted to reduce the value of the correlation function relating fluctuating velocities at subsequent time steps.

8.2 Recommendations for Future Work

While the proposed model of Evinou and Lightstone did not significantly outperform the other stochastic separated flow models featured in this work, there were extenuating circumstances that should be resolved before any firm conclusions on the merits of the model are drawn. The major recommendation for future work is as follows.

1. The model should be tested using better predictions for the flow field solution. In the course of this research, the $k - \epsilon$ model was found to produce better predictions for the flow field solutions of the shear layer experiments. However, it was impossible to generate the Reynolds stresses using the eddy-viscosity assumption in CFX-TASCflow to input into the anisotropic dispersion models due to memory constraints. This problem could be resolved by solving the flow field on a fine mesh, and then interpolating the solution onto a course grid when solving the particle equation of motion during the particle tracking process.

References

AEA. November 2001 Theory documentation. *CFX-TASCflow* **2.11.1**.

BERLEMONT, A., CHANG, Z., & GOUESBET, G. 1998 Particle lagrangian tracking with hydrodynamic interactions and collisions. *Flow, Turbulence and Combustion* **60**, 1–18.

BERLEMONT, A., DESJONQUERES, B., & GOUESBET, G. 1990 Particle lagrangian tracking in turbulent flows. *International Journal of Multiphase Flows* **16**(1), 19–34.

BURRY, D. & BERGELES, G. 1993 Dispersion of particles in anisotropic turbulent flows. *Journal of Multiphase Flow* **19**(4), 651–664.

COIMBRA, C., SHIROLKAR, J. S., & MCQUAY, M. 1998 Modeling particle dispersion in a turbulent, multiphase mixing layer. *Journal of Wind Engineering and Industrial Aerodynamics* **73**, 79–97.

CROWE, C., TROUTT, T., & CHUNG, J. 1996 Numerical models for two-phase turbulent flows. *Annual Review of Fluid Mechanics* **28**, 11–43.

CSANADY, G. 1963 Turbulent diffusion of heavy particles in the atmosphere. *Journal of the Atmospheric Sciences* **20**, 201–208.

DURST, F., MILOJEVIC, D., & SCHONUNG, B. 1984 Eulerian and lagrangian predictions of particulate two-phase flows: A numerical study. *Appl. Math., Modelling* **8**, 101–115.

ELGOBASHI, S., ABOU ARAB, T. ANDRIZK, M., & MOSTAFA, A. 1984 Prediction of the particle laden jet with a two equation turbulence model. *International Journal of Multiphase Flow* **10**, 697–710.

FAN, L. & ZHU, C. 1998 Principles of gas-solid flows. *Cambridge University Press.*

FOX, R. & MCDONALD, A. 1992 *Introduction to Fluid Mechanics*. New York: John Wiley Sons Inc, 4th edition.

GIBSON, M. & LAUNDER, B. 1978 Ground effects on pressure fluctuations in the atmospheric boundary layer. *Journal of Fluid Mechanics* **86**, 491–511.

GOSMAN, A. & IOANNIDES, E. 1983 Aspects of computer simulation of liquid-fueled combustors. *Journal Of Energy* **7**(6), 482–490.

HENNICK, E. & LIGHTSTONE, M. 2000 A comparison of stochastic seperated flow models for particle dispersion in turbulent flows. *Energy and Fuels* **14**, 95–103.

HINZE, J. 1975 Turbulence. *McGraw Hill* **2**.

HISHIDA, K., ANDO, A., & MAEDA, M. 1992 Particle dispersion in turbulent mixing layer. *International Journal of Multiphase Flows* **18**, 182–194.

HUSSEIN, H., CAPP, S., & GEORGE, W. 1994 Velocity measurements in a high-reynolds number, momentum-conserving, axisymmetric, turbulent jet. *Journal of Fluid Mechanics* **258**, 31–75.

LAUNDER, B. & SPALDING, D. 1974 The numerical computation of turbulent flow. *Computer Methods in Applied Mechanics and Engineering* **3**, 269–289.

LAZARO, B. & LASHERAS, J. 1989 Particle dispersion in turbulent, free shear flow. *Seventh Symposium on Turbulent Shear Flows* **15**, 13.1–13.6.

LIGHTSTONE, M. 2001 Self-consistency and the use of correlated stochastic separated flow models to predict particle motion in turbulent flows. *Proceedings of CFD2001* pp. 1–5.

LIGHTSTONE, M. & RAITHBY, G. 1998 A stochastic model of particle dispersion in a turbulent gaseous environment. *Combustion and Flame* **113**, 424–441.

PICART, A., BERLEMONT, A., & GOUESBET, G. 1986 Modelling and predicting turbulence fields and dispersion of discrete particles transported by turbulent flows. *International Journal of Multiphase Flow* **12**, 237–261.

SHIROLKAR, J., COIMBRA, C., & MCQUAY, M. 1996 Fundamental aspects of modeling turbulent particle dispersion in dilute flows. *Progress in Energy and Combustion Science* **22**, 363–399.

SHUEN, J., CHEN, L., & FAETH, G. 1983 Evaluation of a stochastic model of particle dispersion in a turbulent round jet. *AIChE Jl* **29**, 167–170.

WHITE, F. 1991 Viscous fluid flow. *McGraw-Hill Inc.*.

YUU, S., YASUKOUCHI, N., HIROSAWA, Y., & JOTAKI, T. 1978 Particle turbulent diffusion in a dust laden round jet. *The American Institute of Chemical Engineers* **24**(3), 509–519.

ZHOU, Q. & LESCHZINER, M. June 1991a A lagrangian particle dispersion model based on a time-correlated stochastic approach. *Proc. 1st Joint JSME-ASME Fluids Engineering Conf., 4th Symp on Gas-Solid Flow* **ASME/JSME**.

ZHOU, Q. & LESCHZINER, M. Sept 1991b A time-correlated stochastic model for particle dispersion in anisotropic turbulence. *Proc. 8th Symp. on Turbulent Shear Flows* **Munich**, 1031–1036.